www.sciencemag.org/cgi/content/full/science.1213506/DC1

Supporting Online Material for

Evolutionarily Assembled cis-Regulatory Module at a Human Ciliopathy Locus

Jeong Ho Lee, Jennifer L. Silhavy, Ji Eun Lee, Lihadh Al-Gazali, Sophie Thomas, Erica E. Davis, Stephanie L. Bielas, Kiley J. Hill, Miriam Iannicelli, Francesco Brancati, Stacey B. Gabriel, Carsten Russ, Clare V. Logan, Saghira Malik Sharif, Christopher P. Bennett, Masumi Abe, Friedhelm Hildebrandt, Bill H. Diplas, Tania Attié-Bitach, Nicholas Katsanis, Anna Rajab, Roshan Koul, Laszlo Sztriha, Elizabeth R. Waters, Susan Ferro-Novick, Geoffrey C. Woods, Colin A. Johnson, Enza Maria Valente, Maha S. Zaki, Joseph G. Gleeson*

*To whom correspondence should be addressed. E-mail: jogleeson@ucsd.edu

Published 26 January 2012 on *Science* Express
DOI: 10.1126/science.1213506

This PDF file includes:

Other Supporting Online Material for this manuscript includes the following:
(available at www.sciencemag.org/cgi/content/full/science.1213506/DC1)

Materials and Methods

Research subjects

We used standard methods to isolate genomic DNA from peripheral blood of the affected children and family members. Informed consents were obtained from all participating families and the studies were approved by the Casa Sollievo della Sofferenza, and the University of California, San Diego.

Genetic mapping

Genome wide linkage was performed using a 5K Illumina Linkage IVb mapping panel and analyzed with easyLinkage-Plus software. Multipoint LOD scores were calculated using Allegro version 1.2c where parameters were set to autosomal recessive with full penetrance and disease allele frequency of 0.001.

Mutation screening

Bioinformatics strategies involved design of primers to amplify 1643 of the 1667 potential JBTS2 target amplicons from 25 individuals (2 affected and both parents from each of 7 families) resulting in 100% sequence coverage at 1x and 80% sequence coverage at 2x using bidirectional Sanger-based sequencing. The resultant 82,150 sequence reads were annotated according to filters to exclude (1) any polymorphism heterozygous in an affected, (2) any polymorphism reported as homozygous in dbSNP, (3) any polymorphism homozygous in both parents and affected. From this data, we identified *TMEM138* mutations in all remaining JBTS2 families. To test for additional *TMEM138* mutations in a cohort of 460 individuals with JBTS, we applied high-resolution melting using a LightCycler 480 (Roche Applied Science), with the same *TMEM138* primers and optimized PCR conditions. Mutations were validated by Sanger sequencing. All mutations segregated properly according to a single recessive disease mode. All mutations were excluded in 200 Central Asian (predominantly Pakistani and Egyptian) and 200 European (predominantly British) individuals, as well as a cohort of 96 ethnically diverse individuals by Sanger sequencing or high-resolution melting followed by Sanger sequencing. Two mutations were seen in more than one family, correlating with their country of origin, each observed on a shared haplotype. No *TMEM216*-mutated patients had mutations in *TMEM138*, or vice versa, suggesting independent mutational events. The phenotype associated with *TMEM138* mutations is characterized by the presence of the MTI and extreme variability of other ciliopathy features that is characteristic of the JBTS2 locus (Table S1).

Bioinformatics

Genetic location is based on Human Genome Browser build hg18 of the human genome. Genetic locations for the other genomes were obtained from UCSC Genome Browser and Ensemble web site (Table S2-3) (*1*). The conserved genomic regions (>50% sequence similarity) were searched using mVISTA, ECR browser, and PhastCons of UCSC genome browser (*2-4*). Possible regulatory elements were searched using VISTA Browser and ENCODE Regulation database through UCSC Genome Browser (*5, 6*). To predict the protein structure of TMEM138, Phobius and TMHMM web-based tools were

used (*7*). The sequence alignment of TMEM138 and TMEM17/TMEM80/TMEM216 was performed with the Geneious program (http://www.geneious.com). Pairwise alignments of *TMEM138* and *TMEM216* were performed using EMBOSS-Align and BLAST. GeneCards microarray data was obtained from http://www.genecards.org.

Phylogenetic analysis

Phylogenetic analysis was conducted in order to examine the relationships of the TMEM proteins. The identified TMEM138, TMEM216, TMEM80, and TMEM17 proteins were aligned by clustal W using BioEdit Sequence Alignment Editor (*8*). The aligned sequences were manually trimmed on the N- and C-terminal ends to remove weak or ambiguous alignments. Phylogenetic analysis was performed using MEGA4 (*9*). We used default settings for the Neighbor-Joining method (JTT Matrix model). To estimate the reliability of the phylogenetic tree, bootstrap analysis was performed with 500 replicates of full heuristic searches.

Cloning

Full-length *TMEM138* was cloned into the pcDNA3.1 vector and then shuttled into mCherry-, EGFP- and Flag-containing vectors (all tags on C-terminus of *TMEM138*). Mutations were introduced into *TMEM138*-pEGFP-N3 by QuikChange mutagenesis (Stratagene). The *TMEM138* open reading frame was also cloned into pCS2+ vector to make RNA for injection into zebrafish embryos. *TMEM216* related plasmids have been described previously (*10*). Zebrafish orthologs of human *TMEM138* (XM_001333589) and *TMEM216* (XM_678677) was cloned into the pcDNA3.1 and then shuttled into EGFP- and mCherry-containing vector respectively. Myc-*TRAPPC9* and *RFX4*-Flag were gifts from Dr. Ferro-Novick (*11*) and Dr. Peterson (*12*), respectively.

Cells, antibodies, and other reagents

IMCD3, COS7, hTERT-RPE, HEK293T, and ZF4 (zebrafish embryonic fibroblasts) cells were grown in DMEM or DMEM-Ham's F12 supplemented with 10% (vol/vol) fetal bovine serum (FBS) at 37 °C or 30 °C (for ZF4) in 5% CO2. Patient fibroblasts were maintained in MEM supplemented with 20% (vol/vol) FBS. Normal, non-diseased control fibroblasts were from ATCC. Mouse antisera specific to TMEM138 and TMEM216 were raised against the peptide sequence CYFYKRTAVRLGDPHFYQDS (131–150aa) and MLPRGLKMAPRGKRL (1-15aa) respectively by A&G Pharmaceutical Inc. Rabbit anti-TMEM216 antibody has been described (*10*). Primary antibodies used were mouse anti-EGFP antibody (Covance MMS-118R); mouse or rabbit anti-FLAG (Sigma-Aldrich); mouse anti-α-tubulin, (Sigma-Aldrich); mouse anti-glutamylated tubulin (GT335) (*13*); rabbit anti-ADP-ribosylation factor-like 13B (Arl13b) (*14*); rabbit anti-Cep290 (*15*); rabbit anti-γ tubulin (Sigma-Aldrich); rabbit anti-detyrosinated alpha tubulin (glu-tubulin) (Millipore); mouse anti-early endosome antigen1 (EEA1) (BD Bioscience); mouse anti-GM130 (Abcam); rabbit anti-LAMP2 (Abcam); MitoTracker (Molecular Probes). Secondary antibodies were Alexa-Fluor 488-, Alexa-Fluor 594- and Alexa-Fluor 568- conjugated goat anti-mouse IgG and goat anti-rabbit IgG (Molecular Probes), and horseradish peroxidase–conjugated goat anti-mouse and goat anti-rabbit (Dako). Nocodazole was purchased from Sigma-Aldrich.

Biochemical assays

Constructs encoding wild-type or mutants of tagged (EGFP or flag) TMEM138 were transfected into 293T cells. Cells were lysed after 36-48 h and samples analyzed by protein blotting with α-EGFP (1:500), α-TMEM138 (1:1000), α-FLAG (1:2000). Whole-cell extracts were prepared from healthy control and patients fibroblasts in 100-mm tissue culture dishes and analyzed by protein blotting with α-TMEM216 (1:1000) antibody. Normalized loading levels or transfection efficiency were confirmed by blotting with α-tubulin (1:2,000) or the co-transfection with pTK β-gal (1:10 ratio) and subsequent β-gal assay respectively.

Transfection and siRNAs

For transfection with plasmids, cells at 70-80% confluency were transfected using Lipofectamine 2000 (Invitrogen). Cells were incubated for 24-36 h before lysis or immunostaining. For RNA-interference knockdown in IMCD3, hTRET-RPE, and COS7 cells, siRNAs (Table S7 and Fig. S19) were designed against different regions of the human and mouse *TMEM138* and *TMEM216,* human *TRAPPC9, p115,* and *COG1* human *RFX1* to *5*. siGENOME Non-Targeting siRNA pools (Dharmacon) were used as scrambled siRNA controls. Individual siRNAs (20 nM) or siRNA pools (total 60 nM) were transfected into each cells at 30-40% confluency using Lipofectamine 2000 RNAiMAX (Invitrogen). Further assays were carried out 36-48 h after transfection. For the complementation experiments, the cells were co-transfected with an empty or expression vector that expresses myc-*TRAPPC9** and then immunostained 36-48 h later. The vector myc-*TRAPPC9** contains three silent mutations (2558T to G, 2559C to T, 2561C to A) in the CDS region where siRNA1 against human *TRAPPC9* targeted.

In situ hybridization in human embryos

Human embryos were collected from terminated pregnancies using the mefiprestone protocol in agreement with French bioethics laws (94-654 and 04-800). Embryos were fixed in 11% formaldehyde, 60% ethanol and 10% acetic acid, embedded in paraffin and sectioned at 5 µm. *TMEM216* riboprobes used were those described previously (*10*). Primers for *TMEM138* (*TMEM138*F_HIS: TCGAAGGTGACCTCTTGTCA, *TMEM138*R_HIS: TCTGTCCCAGGCTAAAGGAA) were selected on the 3 prime end of the cDNA for PCR amplification on human DNA to be used as template for generating the riboprobes, as described previously (*16*). Sections were hybridized with a Digoxygenin labeled probe at 70°C overnight, and digoxygenin was detected with an anti-DIG-Fab' antibody (Roche) at 1:1000.

Chromatin immunoprecipitation

Chromatin immunoprecipitation (ChIP) assay was performed as described (*17*) with minor modifications. The cross-linked chromatins (first 2mM DSG and then 1% formaldehyde) in hTERT-RPE cells were sheared to ~300-500 bp fragments with a Bioruptor UCD-200TM (Diagenode). The crosslinked adducts extracts were pre-cleared with Precelaring Matrix F (Santa Cruz Biotech) and subsequently incubated with 1-2 ug rabbit IgG or RFX4 antibodies (*18*) overnight at 4 °C and followed by Sepharose A beads for 2 hr. After extensive washing of the beads, DNA-proteins complexes were eluted and crosslinking was reversed overnight at 65 °C. After DNA purification with QIAquick

spin column (Qiagen), real-time qPCR was performed. Primer sets: RE1 #1(F: CAGACAAGGTTGCAGAAAAGC, R:AGGCTCTTTGACTCCCCAAT), RE1 #2 (F: CCTAAAATTCTAGAGTACGGAGAACC, R:GGGCAATGCTTGGATTCTTA), RE2 #1(F:CCAGTATGCAACCCCATTTC, R:TAGTTGCGTGACTTGCCTTG), RE2 #2 (F:TCAAGCCTGTGCTTGTCTTG, R: AGCTCCAATGAAGCCTTGTC), Intergenic control (F:AAAGAGGCGGACAGATGAGA, R: TGCTTCAGTGTGCCTTTGAC)

Immunofluorescence and confocal microscopy

IMCD3, COS7, patient fibroblasts, or hTERT-RPE cells were seeded eight-well microscope chamber slides and fixed in cold methanol (10 min at 4°C) or 4% (vol/vol) paraformaldehyde (10 min at room temperature) depending on antigens. Primary antibodies and Alexa 488- or Alexa 594- or Alexa 647- conjugated secondary antibodies (Molecular Probes) were applied for 1 • h at room temperature. Cells were viewed using a Deltavision deconvolution microscope (100x objective, 1025x1025 resolution with 4x digital magnification for high resolution images) (Applied Precision). For 3D reconstruction, confocal images with Z-stacks were obtained using a Nikon Eclipse TE2000-E system, controlled by EZ-C1 3.50 (Nikon) software. 3D images were processed using Volocity imaging software (PerkinElmer).

Live cell imaging

Cells were seeded at ~30% confluency on eight-well Lab-Tek chambered coverglass (Nunc) and transfected with plasmids or siRNAs for 24 h. Images were acquired for 3-5min with ~3s interval using an Olympus IX70 microscope and a cooled charge-coupled device system with temperature and CO_2 control. For FRAP (Fluorescence recovery after Photobleaching), TMEM216-GFP expressing cells were exposed to the maximum strength of light source for 20min and photobleaching of GFP was confirmed before the acquisition of images for 30min with 30s interval. Acuquired images were deconvolved using Deltavision system (Applied Precision). Numbers of individual vesicles and tethered vesicles were measured using Volocity imaging software (PerkinElmer).

Immunoelectron microscopy

Immuo-EM method has been described previously (*11*). In brief, 293T cell were transfected with *TMEM138*-flag or –EGFP and *TMEM216*-flag or –EGPF for 24h and were fixed by adding 4% freshly prepared formaldehyde. Cells were stored until further processing in 1% formaldehyde at 4°C. Processing of cells for ultrathin cryosectioning and immunolabeling according to the protein A-gold method. The cell pellet was solidified on ice and cut into small blocks. For cryoprotection, blocks were infiltrated overnight with 2.3 M sucrose at 4°C and then mounted on aluminum pins and frozen in liquid nitrogen. To pick up ultrathin cryosections, a 1:1 mixture of 2.3 M sucrose and 1.8% methylcellulose was used. Anti-flag antibody and anti-EGFP antibody were diluted 1:50-1:100. Multiple grids dual-labeled for tagged TMEM138 and TMEM216 were examined and quantitated by electron microscopy. The number of gold particles associated with vesicles and vesiculotubular structures was measured.

Gene expression analyses with quantitative real-time PCR

For the relative quantification of gene expression, we used quantitative real-time PCR for the standard curve method. We collected total RNA from cells and representative tissues of zebrafish and mouse using RNeasy Mini kit (Qiagen). Total RNA (300ng) was reverse-transcribed using the Superscript III first-strand cDNA system (Invitrogen). PCR analysis of cDNA was performed primers (Table S7) specific for human or mouse and zebrafish *TMEM138* and *TMEM216*, human *RFX1* to *5*, human *TRAPPC9* , *p115* and *COG1* after optimization to eliminate primer-dimers and subsequent confirmation by analysis of amplimer dissociation curves after a quantitative PCR run. Each reaction was run in triplicate. Amplimer levels were quantified continuously with the SYBR green Master (Roche) using LightCycler480 instrument (Roche). *β-actin* (for mouse and human), *36B4* (for mouse), or *Rpl13a* (for zebrafish) RNA were amplified for normalization.

Identification of ciliary-defect phenotypes in zebrafish

To knock down *tmem138* or *tmem216 (10)* in wild-type or Tg(*cmlc2:egfp,* a myocardium-specific transgenic reporter line) zebrafish, morpholinos (MO) (Table S7) or control oligonucleotide (Gene Tools) was microinjected (1-6ng) into one- to two-cell-stage embryos, obtained from natural spawning of wild-type (AB) zebrafish lines (for gross morphology and gastrulation) or Tg(*cmlc2:egfp*) zebrafish (for determining L/R axis of heart). The mRNA encoding full-length human *TMEM138* or *TMEM216* was co-injected**.** 3-5 days after fertilization, the morphological phenotypes of morphants were quantified under bright-field microscopy on the basis of ciliary defects (hydrocephalus, pericardial effusion and curved or kinked tail) or embryonic-lethal phenotypes. Morphants at the 9-10 somite stage were scored live according to previously described objective criteria.

RNA in situ hybridization and morphometric analyses

Embryos were fixed at the 9-10 somite stage in 4% paraformaldehyde, hybridized *in situ* with *krox20*, *pax2*, and *myoD* riboprobes according to standard procedures, and flat-mounted for morphometric analyses (n=8-10 embryos/injection batch). Images were captured at 8x magnification on a Nikon AZ100 stereoscope and analyzed with NIS Elements software

SOM text

Coordinated expressions of adjacent TMEM138 and TMEM216 mediated by non-coding intergenic region

We found two candidate REs, RE1 and RE2 with conserved DNaseI hypersensitive sites located in the dips surrounded by H3K4 monomethylation (H3K4me1) peaks (*19*), suggesting that DNA binding factors might regulate the transcription of these two genes (Fig. S7A-B). Regulatory factor X (RFX) paralogues binding to symmetrical X-box DNA elements are known to transcriptionally regulate genes necessary for ciliary formation (*12, 20*), and we found that the REs contained X-box consensus sequence motifs (Fig. S7B). Using knockdown, overexpression, and chromatin immunoprecipitation experiments, we further found that among the five known mammalian RFXs, RFX4 serves in transcriptional activation, associating with RE2 to mediate coordinated expressions of *TMEM138* and *TMEM216* (Fig. S7C-E).

TMEM138 and TMEM216 vesicles differentially associate with cilia-targeted proteins

Meckelin, a ciliary protein required for ciliogenesis was reported to interact with TMEM216 (*10*). Among other ciliary proteins, CEP290, controlling flagella protein content and crucial for ciliary formation, is known to localize at the transition zone and pericentriole matrix of cilia where TMEM138 is localized but where TMEM216 is adjacent (Fig. 3B and Fig. S9C) (*15, 21*), making it a good candidate for TMEM138 cargo. We indeed found that CEP290 specifically localized with TMEM138 vesicles (Fig. S13A), but not TMEM216. This data suggests that that TMEM138 and TMEM216 mark two distinct but linked vesicle pools, each associated with unique cilia-targeted proteins.

TRAPPII mediates tethering of TMEM138 and TMEM216 vesicles crucial for ciliary assembly

Among potential tethering proteins related to tethering of Golgi vesicles, TRAPPC9 (a core subunit of TRAPPII complex) is uniquely known to be mutated in a recessive human disease, and phenocopies some aspects of Joubert syndrome including cerebellar affection and mental retardation, making it a good candidate for linking the two TMEM proteins (*22*). We genetically tested each of these potential tethering proteins using siRNAs. We found that the siRNA disruption of *TRAPPC9* de-tethered the two vesicular pools (Fig. 4A and Fig. S15A; Movie S7-10). As expected, this resulted in defects of ciliary assembly (Fig. S14C and Fig. S15B). Then, we tested whether the TRAPPII complex localizes where both TMEMs meet using aTRAPPC10 antibody, another core subunit of TRAPPII complex known to interact with TRAPPC9 (*11*). We found that TRAPPC10 overlaps where TMEM138 and TMEM216 signal is adjacent, as one might expect from a tethering protein, suggesting that TRAPPII or components thereof mediate tethering of TMEM138 and TMEM216 vesicles (Fig. S16). Our findings suggest that TRAPPII mediated tethering of TMEM138 and TMEM216 is crucial for ciliary assembly.

Supplemental Figures

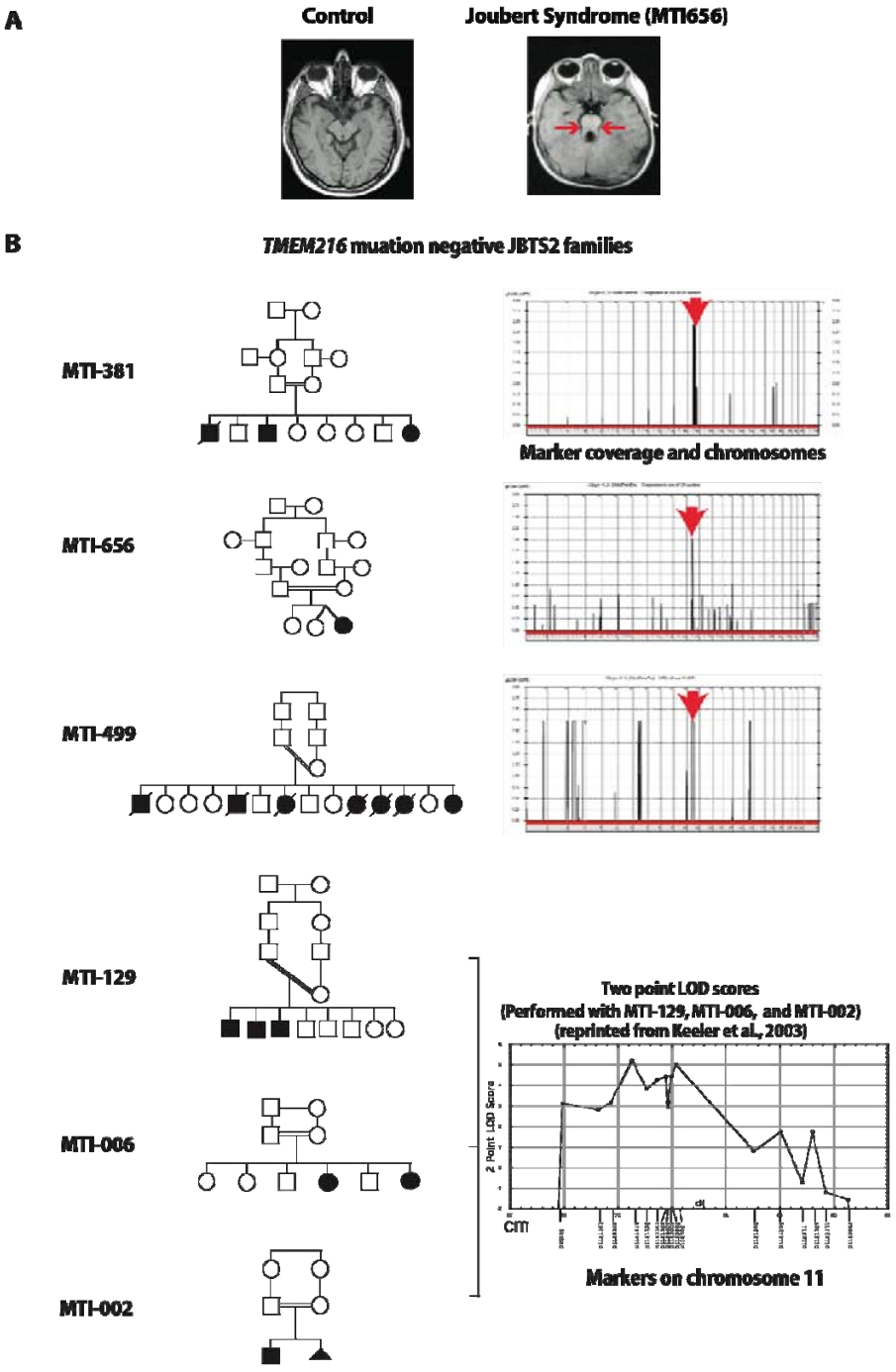

Fig. S1 *TMEM216* mutation negative Joubert syndrome (JBTS) families, which link to JBTS2 locus. (A) Axial brain MRI of a 1-year-old affected female (MIT-656) with a *TMEM138* mutation (p.A126T) shows the pathognomic 'molar tooth' sign (red arrow)

indicating cerebellar malformation in JBTS. (B) Pedigrees of 6 JBTS families negative for *TMEM216* mutations and their linkage plots used in this study are shown. Double bar indicates documented consanguinity. Male=square, Female=circle, Termination of pregnancy=triangle, Hashed line=deceased. LOD score plots present chromosome along x-axis and multipoint pLod along y-axis, as calculated by Allegro v1.2c. Note peak on chromosome 11 in all families.

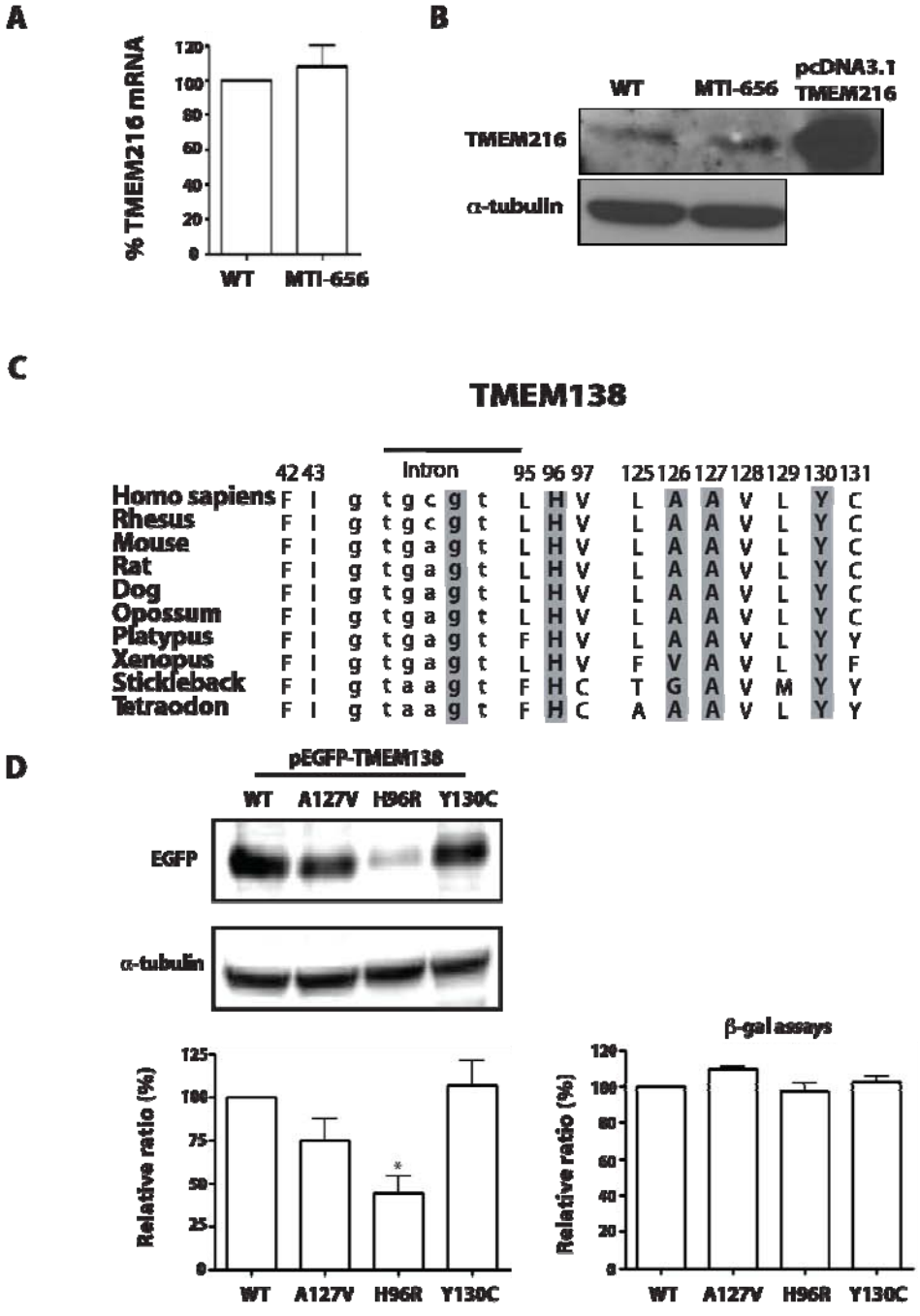

Fig. S2 Genetic heterogeneity at JBTS2 locus and homozygous deleterious mutations of *TMEM138*. (A) Real-time qPCR of patient fibroblasts (MTI-656) and (B) Western blot analysis of whole lysates shows that *TMEM216* mRNA and protein expressions are intact, implying the genetic heterogeneity at JBTS2 locus. Lysates from pcDNA3.1-*TMEM216* expressing HEK293T cells were used as a positive control. (C) Missense and splicing mutation sites of *TMEM138* found in JBTS2 linked families are evolutionary

conserved residues. (D) Shown is a protein blot of whole lysates of HEK293T cells transfected with a cDNA encoding wild-type TMEM138 or one of the missense mutations found in affected individual. Proteins levels were measured by densitometer. α-tubulin blot and β-gal assays (co-transfection with pTK β-gal at 1:10 ratio) were used for normalization of loading and transfection efficiency, respectively. Note that TMEM138 p.H96R resulted in the production of ~40% of wild-type protein level. *$p<0.05$ (*vs* WT by one-way ANOVA with Bonferroni posttest, n=4)

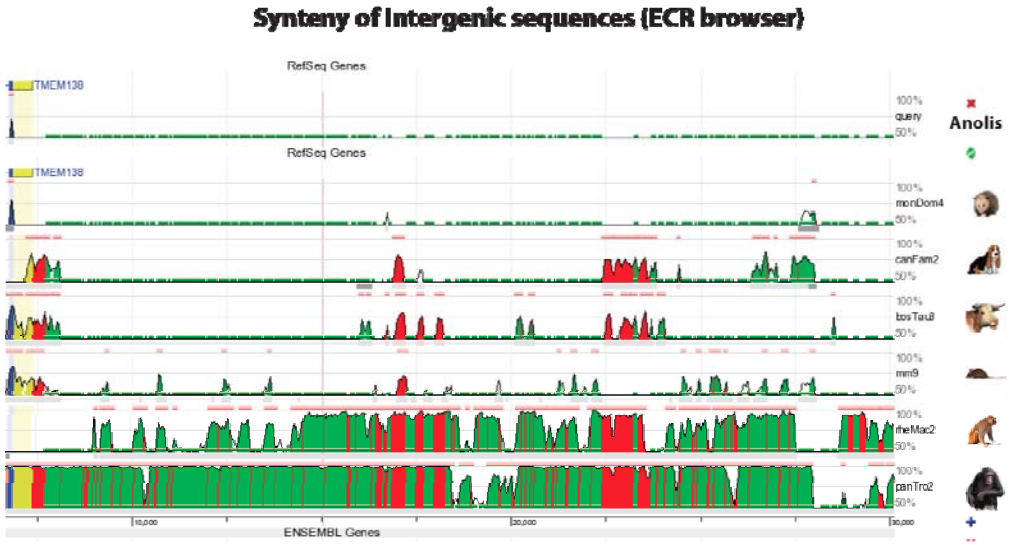

Fig. S3 Synteny of intergenic sequences between *TMEM138* and *TMEM216* using ECR Browser. The conservation profiles of human in comparison with chimpanzee, monkey, mouse, cow, dog, opposum, and anolis (submitted sequences based on coordinates of *TMEM138* and *TMEM216* homologs) are shown. Each line represents an ungapped alignment with the vertical height indicating the nucleotide identity. Pink bars of every layer show evolutionary conserved regions. Conserved alignment is red: intergenic region, green: transposons and simple repeats, yellow: UTRs, and blue: coding exons.

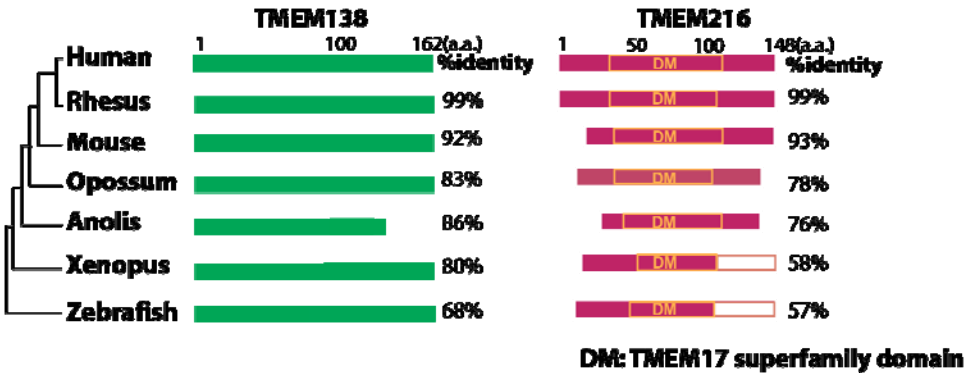

Fig. S4 TMEM138 and TMEM216 protein homologs. The schematic picture shows conserved protein regions (white regions: <50% sequence similarity to human) and percent protein homology to human (Table S4-6). DM: TMEM17 superfamily domain.

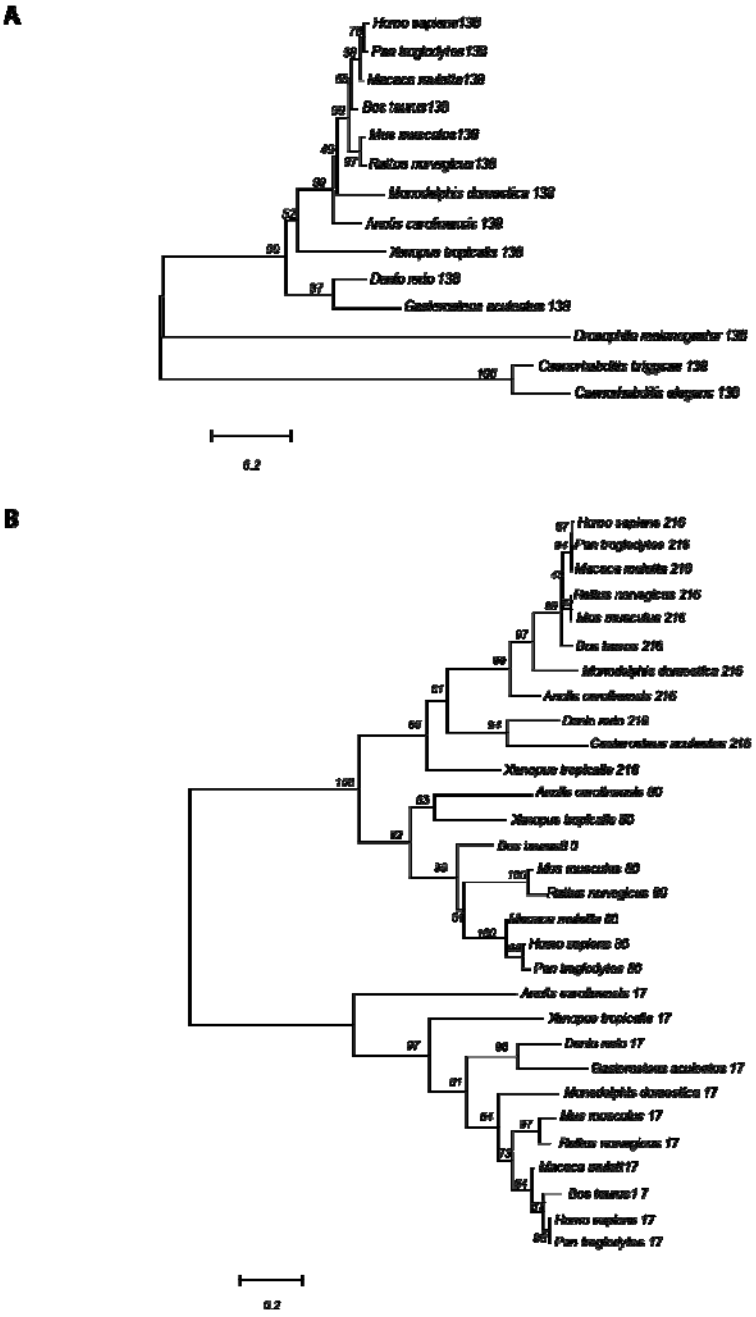

Fig. S5 Phylogenetic trees of TMEM138 and TMEM216 based on amino acid sequence. (A) TMEM138 tree shows that TMEM138 is well conserved throughout species and that the TMEM138 proteins are orthologous. (B) Phylogenetic tree shows TMEM216 and TMEM80 are duplicated from TMEM17 and all consist of the same family sharing a transmembrane 17 superfamily domain. Relationships among the TMEM216 proteins indicate that the proteins are direct orthologs, i.e. there is no

evidence of gene duplication creating paralogous proteins. Scale bar represents the average number of substitutions per amino acid residue. Confidence measurements from bootstrap analysis (500 iterations) are shown in nodes of trees. 216,TMEM216; 17,TMEM17; 80,TMEM80; 138,TMEM138.

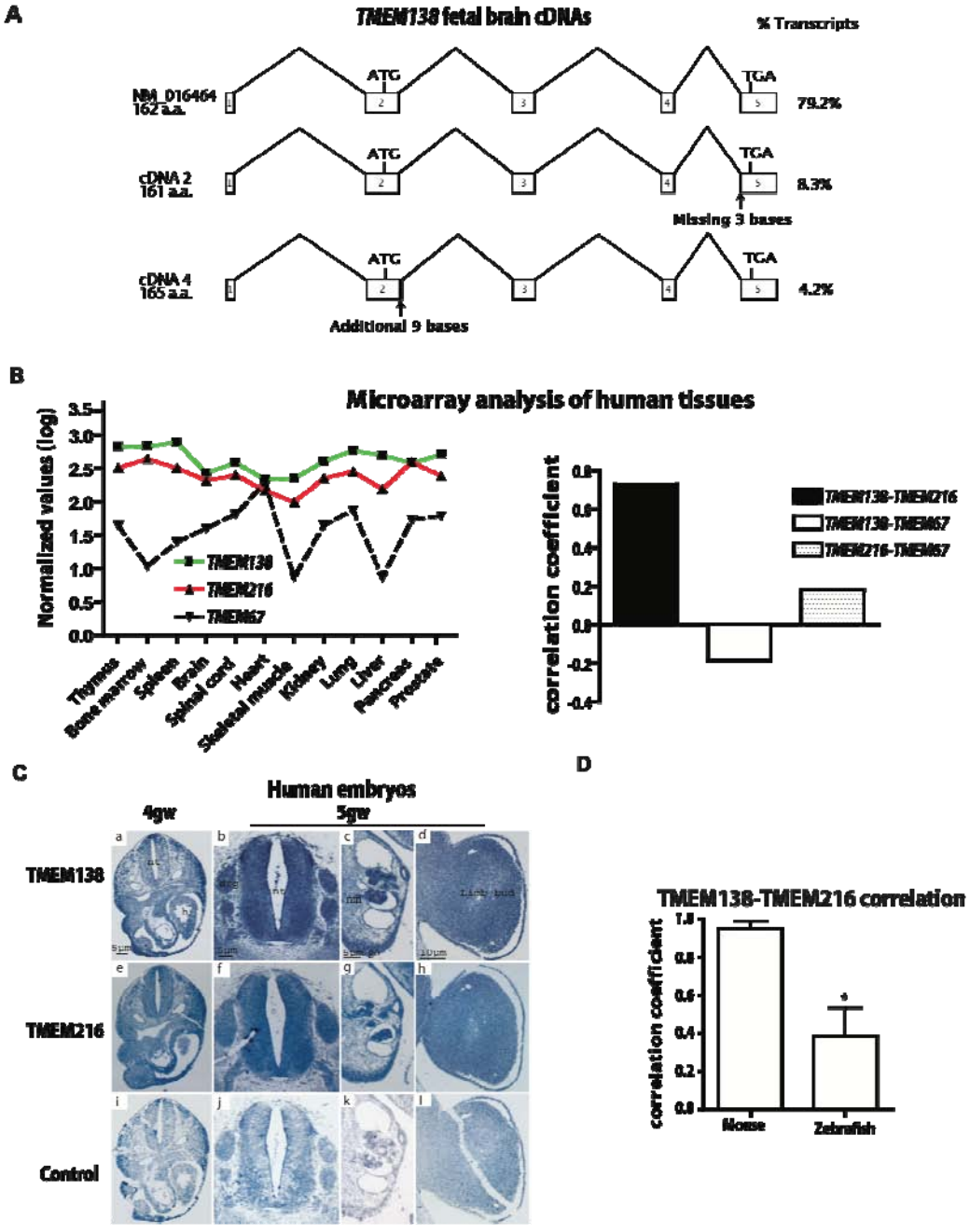

Fig. S6 Coordinated expression of adjacent *TMEM138* and *TMEM216*. (A) Representation of recovered *TMEM138* isoform clones (n=48) from 20 gw human fetal brain cDNA. Single major isoform (NM_016464) was identified and encoded a predicted protein of 162 aa. (B) GeneCards Database(*23*) of human gene expression profile shows similar expression patterns of *TMEM138* and *TMEM216* in representative tissues. The correlation coefficient of represented gene pairs suggests that the expression patterns of

TMEM138 and *TMEM216* in human tissues are highly correlated, compared to *TMEM67*, another known JBTS causative gene (*24*). (C) Similar expression patterns of *TMEM138* and *TMEM216 based* upon *in situ* hybridization in human embryonic tissues. *TMEM138* antisense (a-d), *TMEM216* antisense (e-h) and sense *TMEM138* control probes (i-l). At 4gw, transverse sections show that *TMEM138* as well as *TMEM216* are ubiquitously expressed within embryonic tissues (nt: neural tube, h: heart primordium) (a, e, and i). At 5gw *TMEM138* and *TMEM216* expression became more intense particularly in neural tube (nt), dorsal root ganglia (drg), mesonephros (mn), gonadal ridge (go) and limb bud (b-d and f-h). (D) Real-time qPCR of *TMEM138* and *TMEM216* mRNA in tested tissues of mouse and zebrafish indicates that the average correlation coefficient in mouse (r=0.984) compare to those of zebrafish (r=0.386). *p<0.05 (by Student's t-test, three independent experiments)

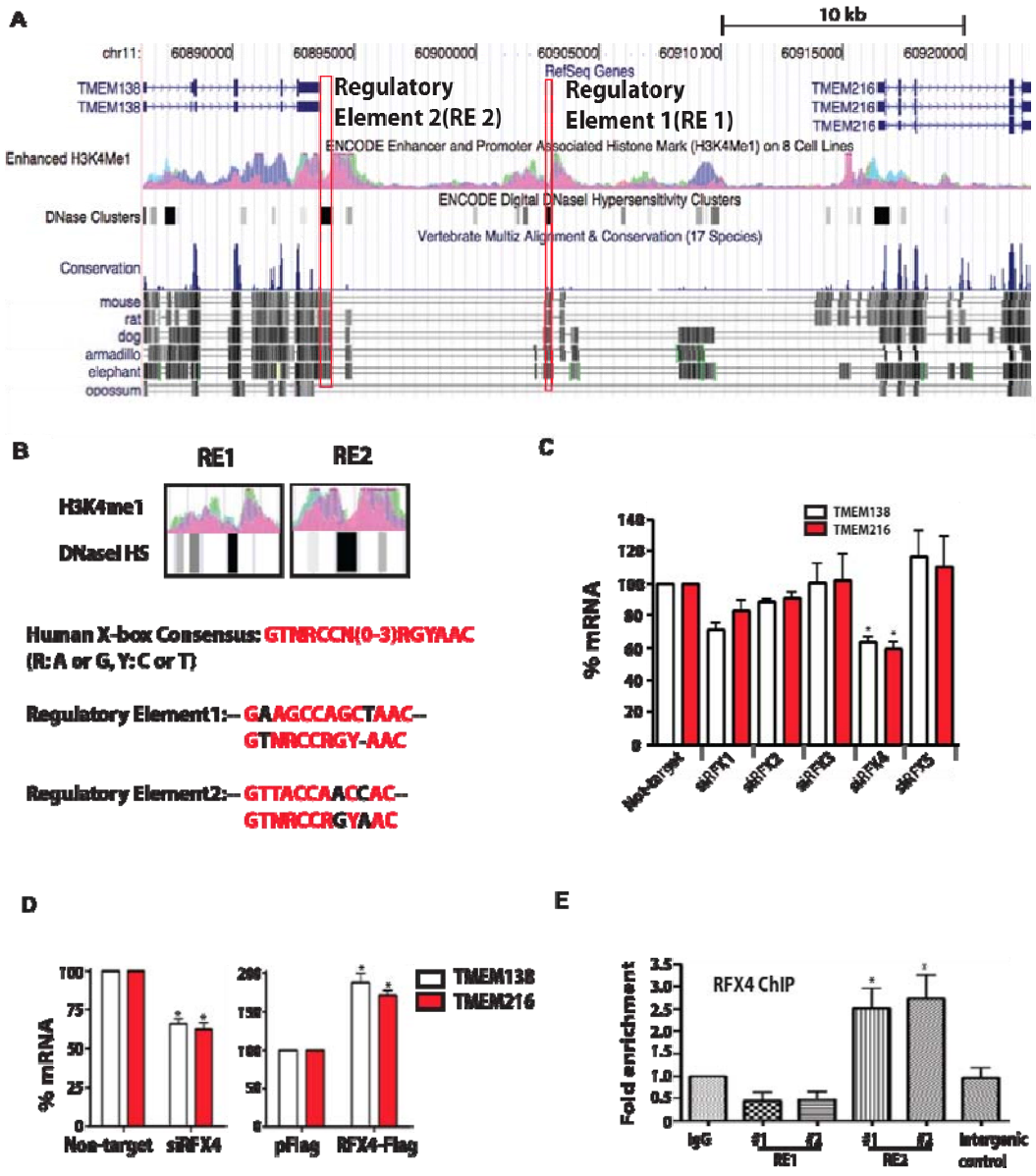

Fig. S7 Coordinated expressions of adjacent *TMEM138* and *TMEM216* mediated by non-coding intergenic region. (A) UCSC genome browser shows possible regulatory elements (RE1 and RE2) in the non-coding intergenic region, which are evolutionarily conserved and DNaseI hypersensitivity clusters. The shading is proportional to the maximum signal strength observed in any cell line. (B) RE1(~200bp) and RE2(~400bp) located in the dips surrounded by H3K4 monomethylation (H3K4me1) peaks contain X-box consensus

sequences for regulatory factor X (RFXs) binding. (C) Real-time qPCR in human ciliated cells (hTERT-RPE) shows that among five *RFX* genes (*RFX1-5*), the knockdown of *RFX4* induced the coordinated decrease of transcriptional expression of both *TMEM138* and *TMEM216* gene. **p*<0.05 (vs Non-target by one-way ANOVA with Bonferroni posttest, n=4) (D) Real-time qPCR in human ciliated cells (hTERT-RPE) shows knockdown of *RFX4* and overexpression of *RFX4*-flag induced the coordinated decrease or increase of transcriptional expression of both *TMEM138* and *TMEM216* gene, respectively. **p*<0.05 (vs Non-target or pFlag by Student's t-test, n=3-4). (E) ChIP assay in hTERT-RPE shows RFX4 binding to RE2 was enriched. #1 and #2 indicate two different primer sets of each genomic region. Non-specific intergenic region between RE1 and RE2 was used as a negative control. * *p*<0.05 (vs IgG by one-way ANOVA with Bonferroni posttest, n=3).

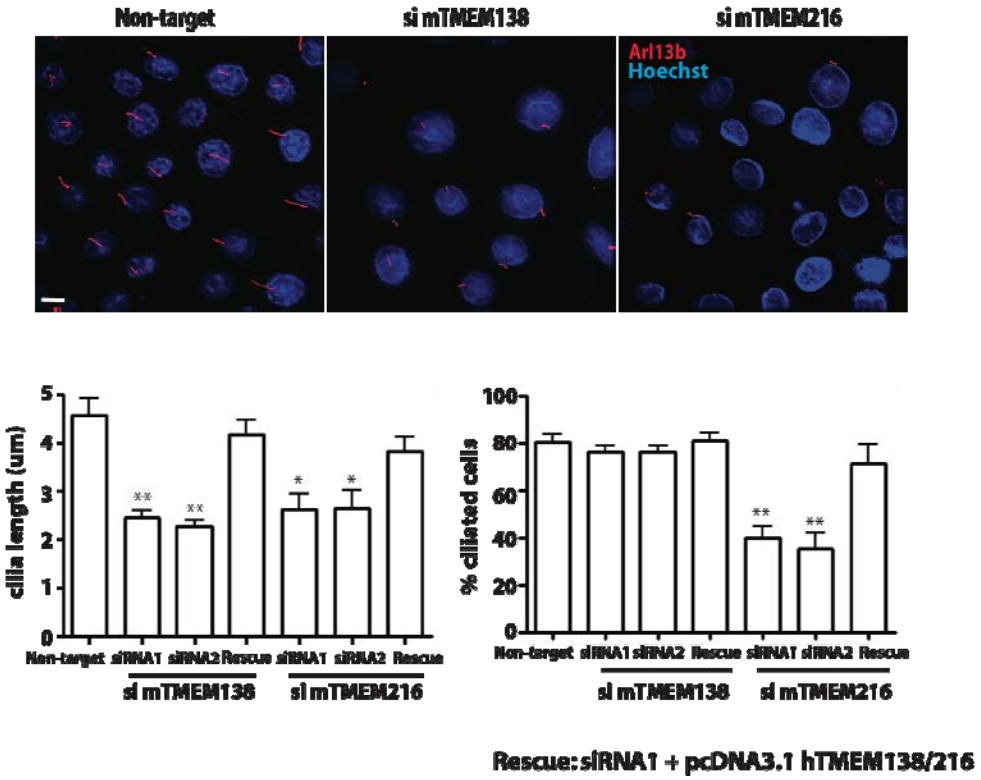

Fig. S8 Knockdown of *TMEM138* and *TMEM216* in IMCD3 cells causes short cilia and defects in ciliogenesis (defined as having cilia <1 μm long). * $p<0.05$, ** $p<0.01$ (vs Non-target by one-way ANOVA with Bonferroni posttest, n=60-70). Scale bars, 5um.

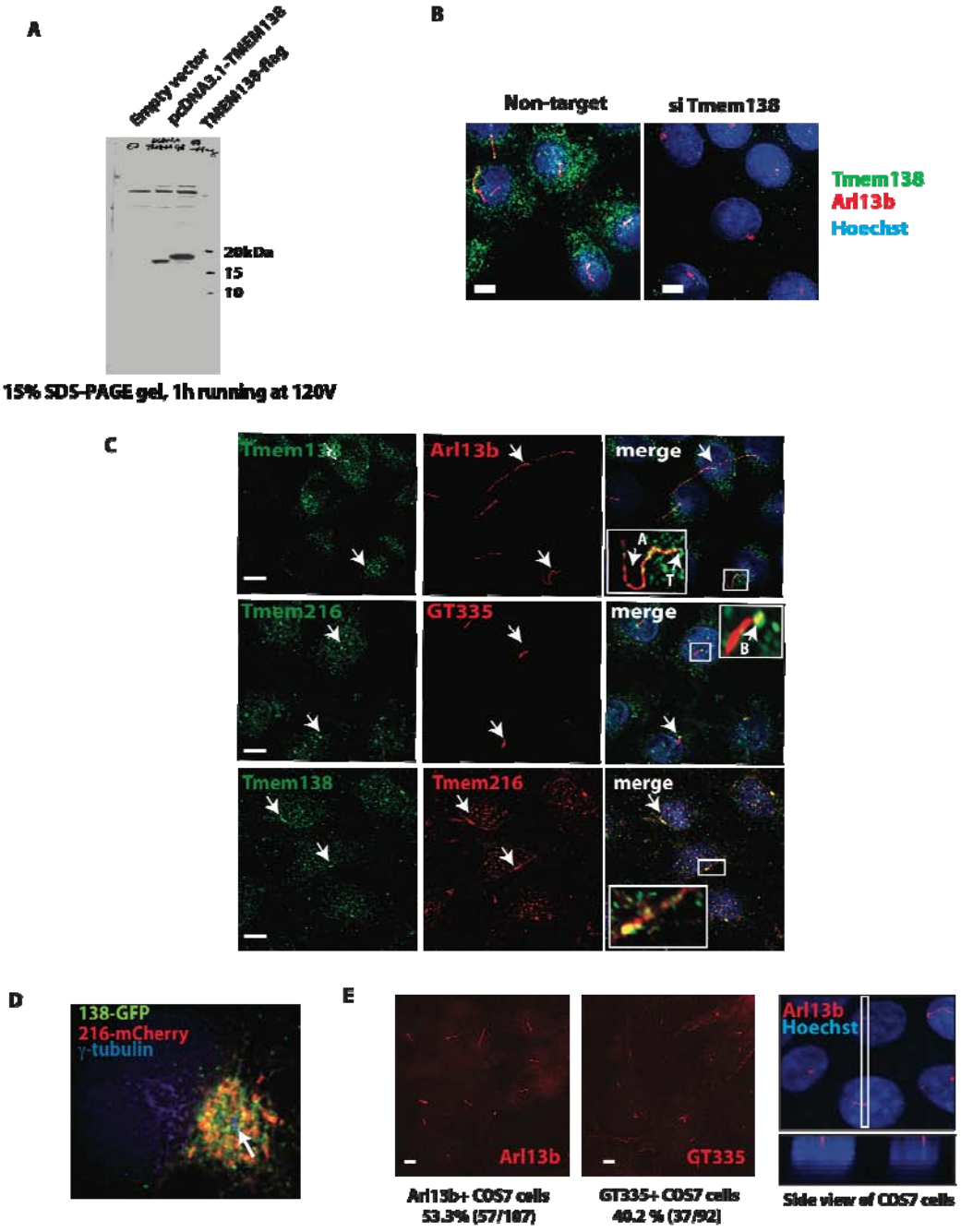

Fig. S9 Adjacent localization of TMEM138 and TMEM216 in IMCD3 and ciliated COS7 cells. (A) Western blot analysis of whole lysates from pcDNA3.1-*TMEM138*, pcDNA3.1-*TMEM138*-flag, and empty vector transfected HEK293T cells and (B) immunostaining of endogenous Tmem138 in *Tmem138* knockdown IMCD3 cells (with shorter cilia) show specificity of generated mouse polyclonal TMEM138 antibody. The protein size of human TMEM138 is ~18kDa. (C) In IMCD3 cells, endogenous Tmem138 or Tmem216

were stained for cilia (Arl13b) or cilia plus centrosome (GT335), indicating the localization of Tmem138 in the ciliary axonem/basal body and Tmem216 in the basal body, respectively. Double labeling shows adjacent vesicular pattern of Tmem138 and Tmem216. A: ciliary axoneme, T: transition zone, and B: basal body. (D) h*TMEM138*-EGFP and h*TMEM216*-mCherry expressing COS7 cells show non-overlapping but closely adjacent vesicular patterns of surrounding the centrosome (γ-tubulin). (E) After 4h serum starvation, COS7 cells (>80-90% of confluence) were stained with ciliary markers (Arl13b and GT335), indicating that 40-50% cells display evidence of cilia. The side view (corresponding to the white box in XY plane view) of cilia in nuclear-labeled cells was shown. Boxes show insets at high power. Scale bars, (B), (C), and (E), 5um.

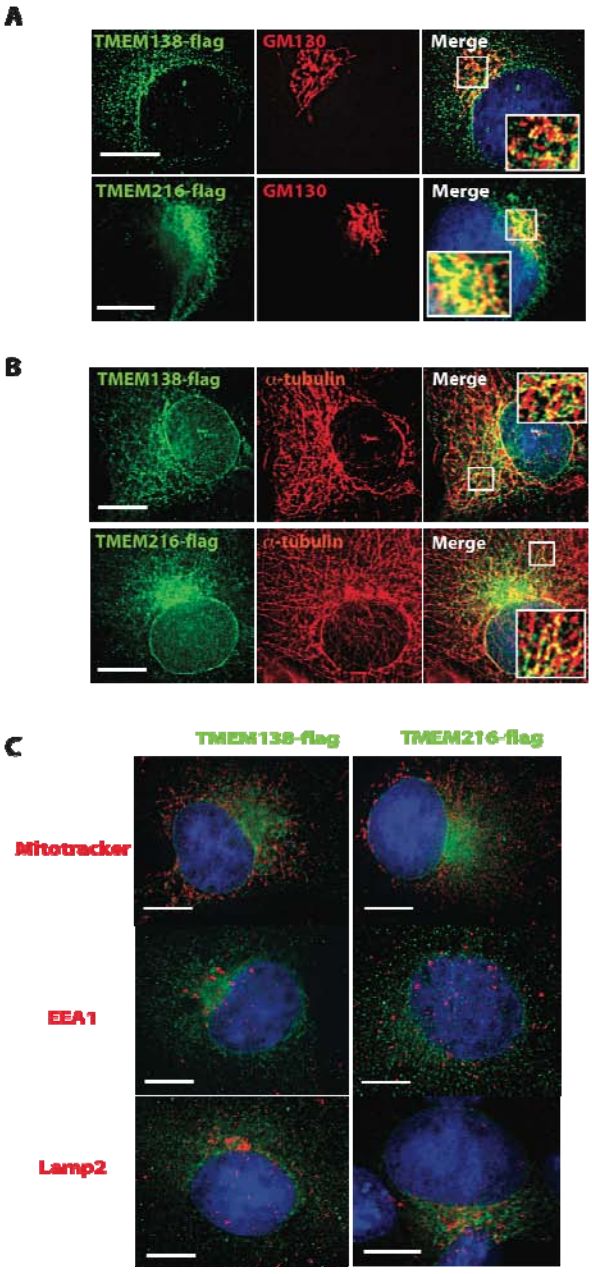

Fig. S10 Subcellular localizations of TMEM138 and TMEM216. Immunostaining in TMEM138-flag or TMEM216-flag expressing COS7 cells with various intracellular organelle markers including Golgi apparatus (GM130), microtubule (α-tubulin), mitochondria (Mitotracker), early endosome (EEA1), and late-endosome (Lamp2). TMEM proteins showed Golgi patterns (A) (also see Fig. S11) and aligned with microtubules (B). However, mitochondria, early-endosome, late-endosome marker did not overlap with TMEM138-flag and TMEM216-flag (C). Boxes show insets at high power. Scale bars 5um.

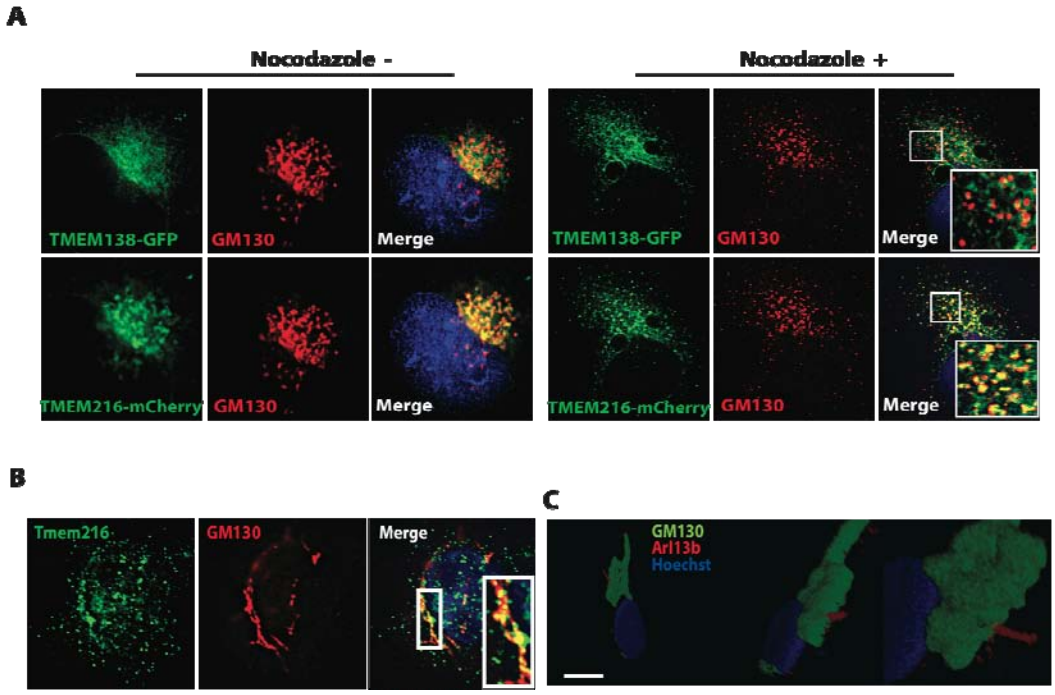

Fig. S11 The localization of TMEM216 with Golgi apparatus surrounding the base of cilium. (A) After 20uM of nocodazole treatment for 1h to disassemble Golgi apparatus complex in TMEM138-GFP and TMEM216-mCherry expressing COS7 cells, TMEM216 co-localized with Golgi marker (GM130) and TMEM138 was adjacent to GM130 in the same cell. TMEM216-mCherry was pseudo-colored as green. (B) Endogenous Tmem216 in IMCD3 cells localized to Golgi apparatus (GM130). (C) The 3D reconstruction of confocal images in hTRET-RPE cell shows that the base of primary cilia (Arl13b) is embedded by Golgi complex (GM130). Boxes show insets at high power. Scale bars 5um.

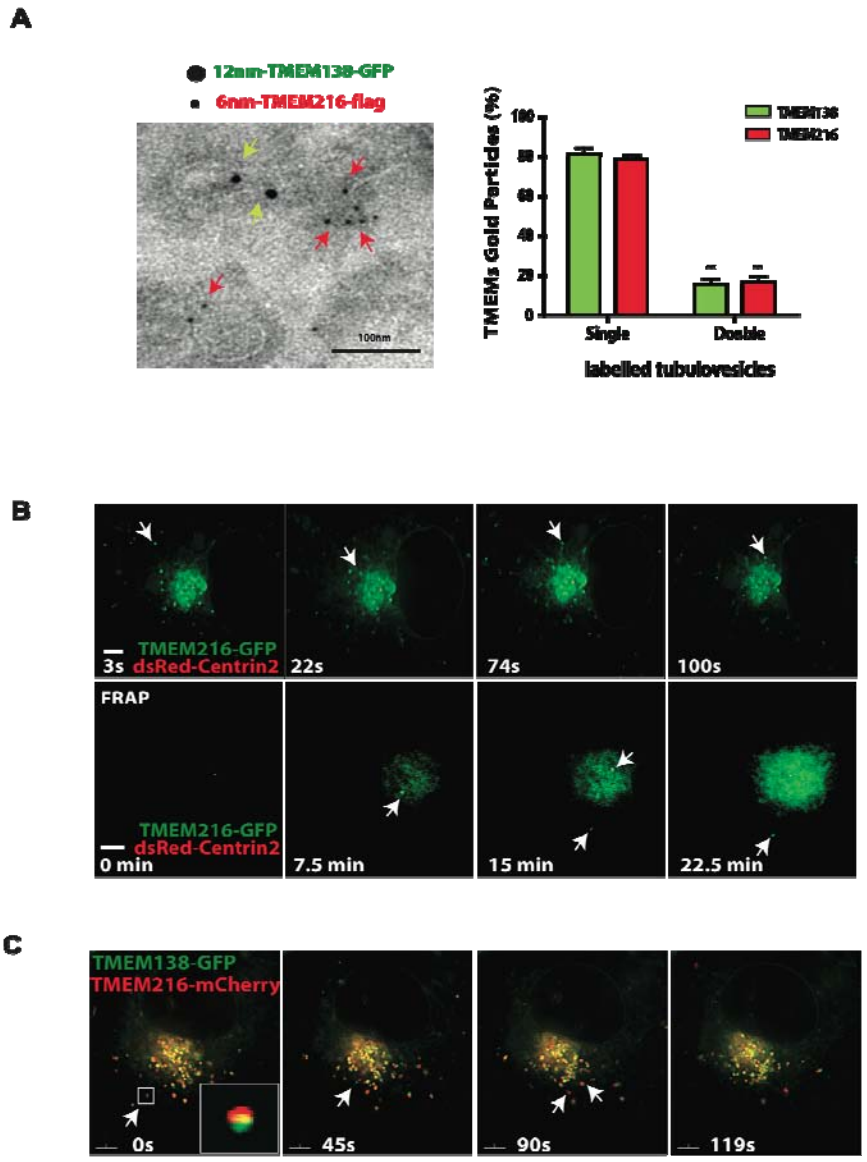

Fig. S12 TMEM138 and TMEM216 marked two distinct vesicular pools moving toward primary cilia. (A) Immunoelectron microscopy analysis in TMEM138-GFP and TMEM216-flag expressing HEK293T cells showing TMEM138 and TMEM216 are on adjacent but unique vesicles. Two 12nm gold particles (green arrows) tagging a TMEM138 containing vesicle are adjacent but not overlapping with six 6nm particles (red arrows) tagging TMEM216. Quantification from vesicles with two or more particles shows predominance of a single TMEM. $^{**}p<0.001$(vs Single by Student's t-test, n>270). (B) In COS7 cells producing primary cilia (Fig. S9E), live cell imaging and fluorescence recovery after photobleaching (FRAP) show that TMEM216-tagged vesicles move toward the centrosome (Centrin2, the central part of the basal body) and the accumulation of GFP signal around it, indicating that the net flux of vesicles is toward the centrosome (Movie S1 and S2). Arrows indicate existing or newly emerging vesicles that move toward the centrosomal marker. (C) Notably, TMEM138 and TMEM216 show

adjacent vesicles that moved together in a hand-in-hand fashion (Movie S3), consistent with adjacent vesicular movements in other ciliated cells (hTERT-RPE) (Movie. S4). Arrows indicate examples of vesicles moving in a hand-in-hand fashion. Boxes show insets at high power. Scale bars, 5um.

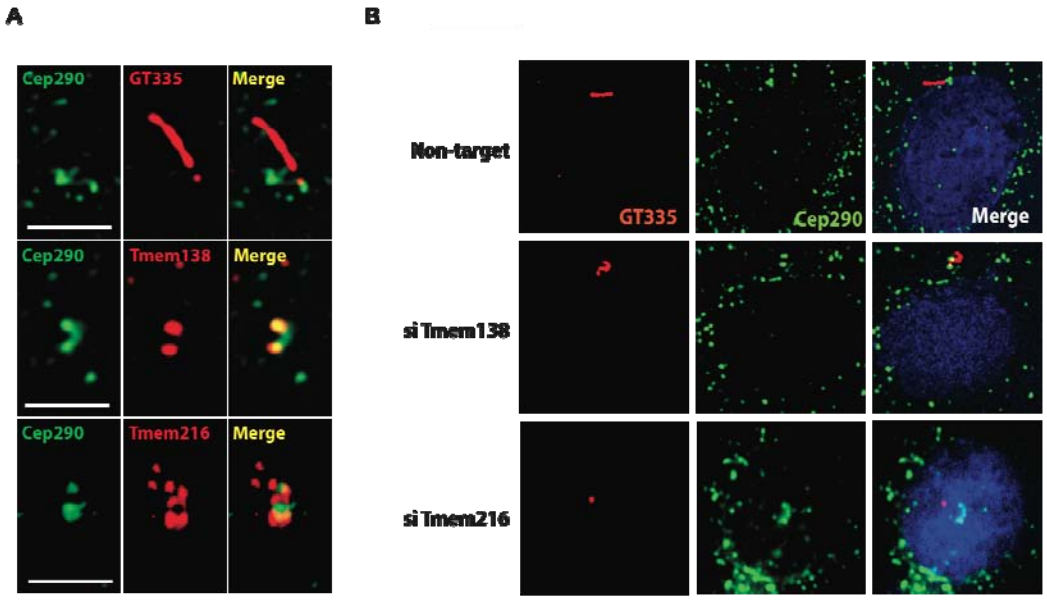

Fig. S13 Tmem138 and Tmem216 vesicles differentially associate with Cep290. (A) Visualized endogenous Cep290 together with cilia plus centrosomal marker (GT335), indicating the pericentrosomal location of Cep290 in IMCD3 cells. Cep290 has overlapping localization with Tmem138, whereas it is adjacent to Tmem216. (B) The knockdown of *Tmem216*, but not *Tmem138* disrupts the trafficking of Cep290 to the base of cilia. Tmem138 is not necessary for Cep290 trafficking. Scale bar (A) and (B) 5um.

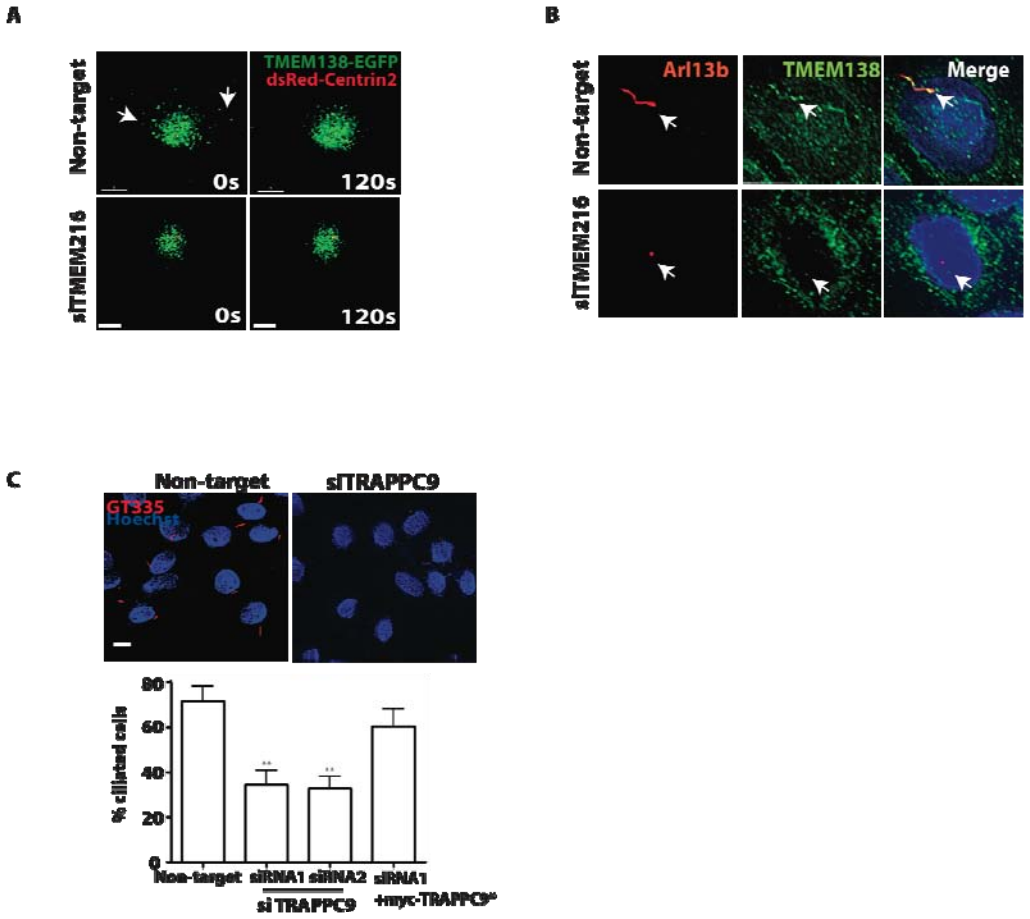

Fig. S14 Functional relatedness of TMEM138 and TMEM216. (A) Live cell imaging in TMEM138-GFP expressing COS7 shows that TMEM216 knockdown severely disrupts TMEM138 vesicular movements. Arrows indicate vesicles moving toward the centrosomal marker (Movie S5-6). (B) Immunostaining of Tmem138 in IMCD cells show that Tmem216 knockdown severely disrupts Tmem138 vesicular trafficking to the primary cilium. Arrows indicate intact or disrupted cilia. (C) In hTERT-RPE cells, knockdown of *TRAPPC9* disrupted ciliogenesis induced by 24h serum starvation and largely rescued by myc-*TRAPPC9** (*see materials and methods*). ** $p<0.01$, ***$p<0.001$ (by one-way ANOVA with Bonferroni posttest, n=90-110). Scale bars, (A) to (C), 5um.

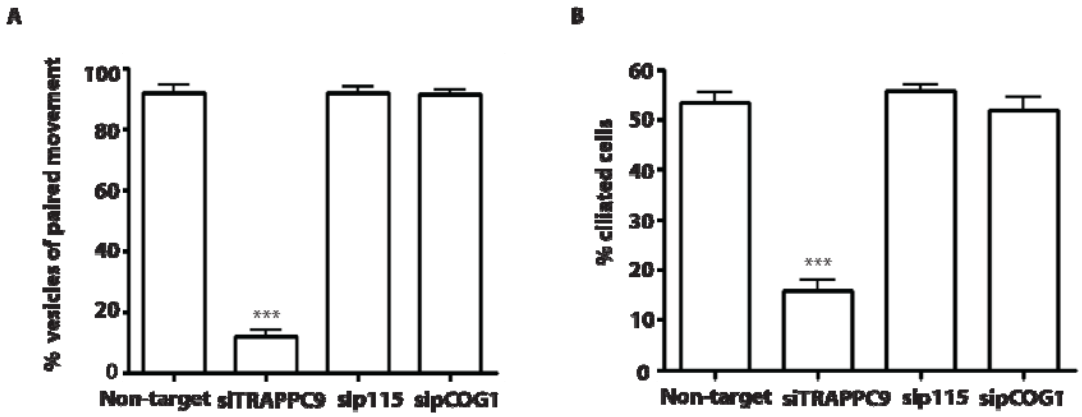

Fig. S15 Effect of *p115* and *COG1* versus *TRAPPC9* knockdown on TMEM138 and TMEM216 vesicular tethering and ciliogenesis. (A) Live cell imaging shows that knockdown of *p115* and *COG1* do not significantly affect vesicular tethering of TMEM138 and TMEM216 in transfected COS7 cells (Movie S9 and 10). (B) In hTERT-RPE cells, knockdown of *p115* and *COG1* do not significantly affect ciliogenesis induced by 24h serum starvation. Both effects were prominently disrupted following TRAPPC9 knockdown.

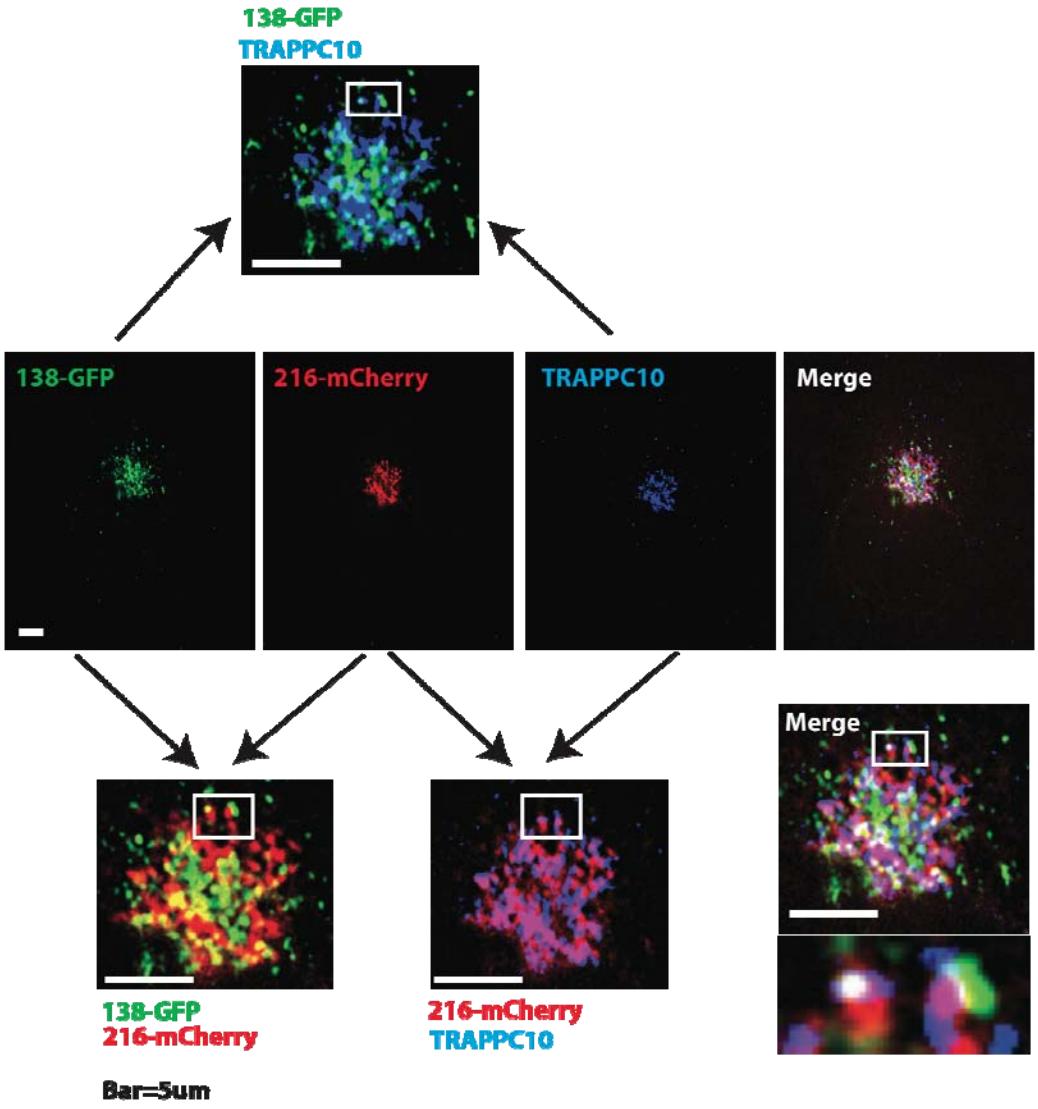

Fig. S16 TRAPPII localizes where TMEM138 and TMEM216 vesicles are adjacent. Endogenous TRAPPC10 (blue), a major subunit of TRAPPII, was stained in TMEM138-GFP (green) and TMEM216-mCherry (red) expressing COS7 cells. Images of each pair of colors presented. Merged image showed that white signal are strong at sites where green (TMEM138) and red (TMEM216) vesicles adjacent, indicating that TRAPPC10 overlays the adjacency of TMEM138 and TMEM216. Scale bar, 5um.

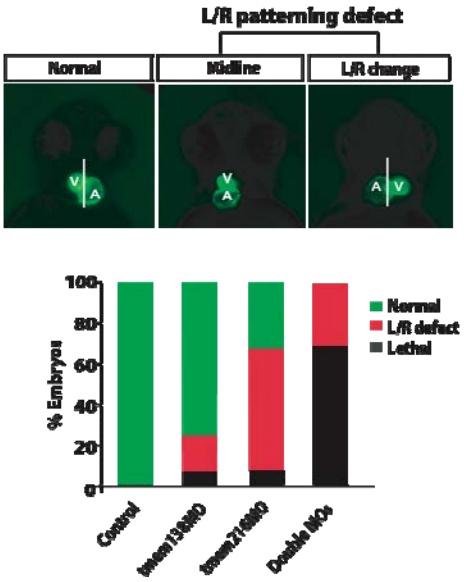

Fig. S17 Defects of L/R heart axis in *tmem138* and *tmem216* morphants. Injection of MOs in Tg(*cmlc2:egfp*) zebrafish embryos shows more severe L/R patterning defects of heart in *tmem216* morphants than *tmem138* (>50 embryos each condition).

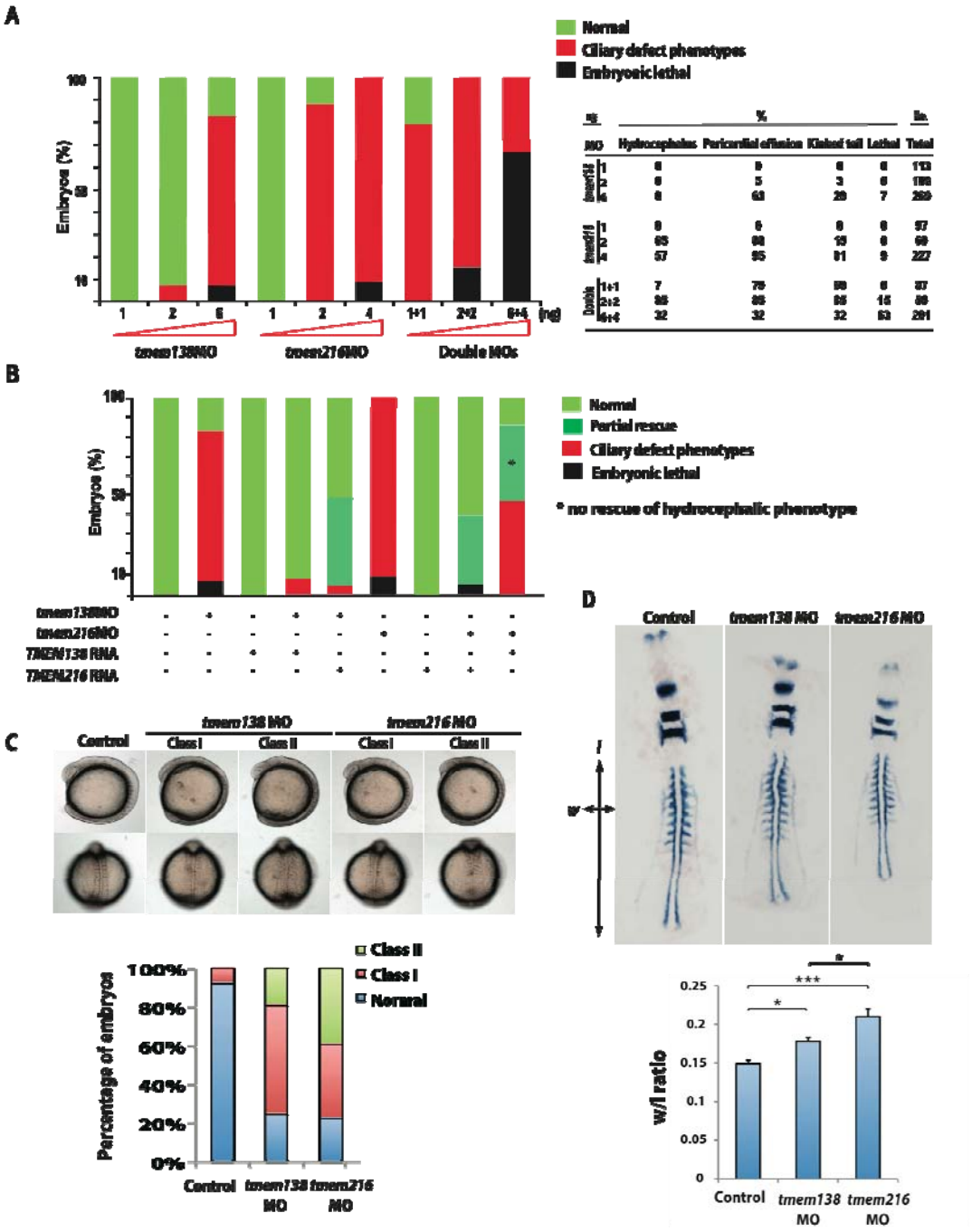

Fig. S18 Analysis of *tmem138* and *tmem216* morphants. (A) Injection of translation-blocking antisense morpholinos (MO) to *tmem138*, *tmem216*, or double in wild-type (AB) zebrafish embryos caused ciliary phenotypes including hydrocephalus (only in *tmem216* morphants), pericardial effusion, kinked tail, and lethality at 3 days post fertilization in a synergistic and dose-dependent manner. (B) *tmem138* or *tmem216* morphant phenotypes were mostly rescued by co-injection of RNA encoding human

TMEM138 or *TMEM216*. Trans-rescues showed that *tmem138* morphants were largely rescued by *TMEM216 RNA*, whereas *TMEM138 RNA* did not effectively rescue tmem216 morphants (especially, hydrocephalus phenotypes). Trans-rescues by cognate human RNA showed some functional redundancy of *TMEM216* in *tmem138* morphants but not *vice versa*. "Partial rescue" means any remaining of weak ciliary defect phenotypes (i.e. mild curved tail). (>50 embryos each condition). (C) At early stage of zebrafish embryos (9-10 somites), MO-based suppression of *tmem138* or *tmem216* give rise to similar gastrulation defects quantified based on previously described objective criteria. Class I, shortened body axis, small anterior structures, broad somites; Class II, severely shortened anterior-posterior axis, small anterior structures, severely broadened somites with kinking of the notochord. Representative lateral (top panels) and dorsal (bottom panels) views of live embryos are shown. n=55-81 embryos/injection batch with masked scoring, repeated twice with similar results. (D). Whole embryo flat mounts hybridized *in situ* with a cocktail of *krox20*, *pax2*, and *myoD* riboprobes. Morphometrics demonstrate phenotypic defects in two different axes of development. w, width spanning the lateral ends of the fifth appreciable somites counted from the anterior end of the embryo; l, length of the notochord as indicated by adaxial cell labeling; w/l, ratio of measurements is indicated, n=8-10 embryos/injection batch. P-values denoted as * ($P<0.01$) or *** ($P<0.0001$).

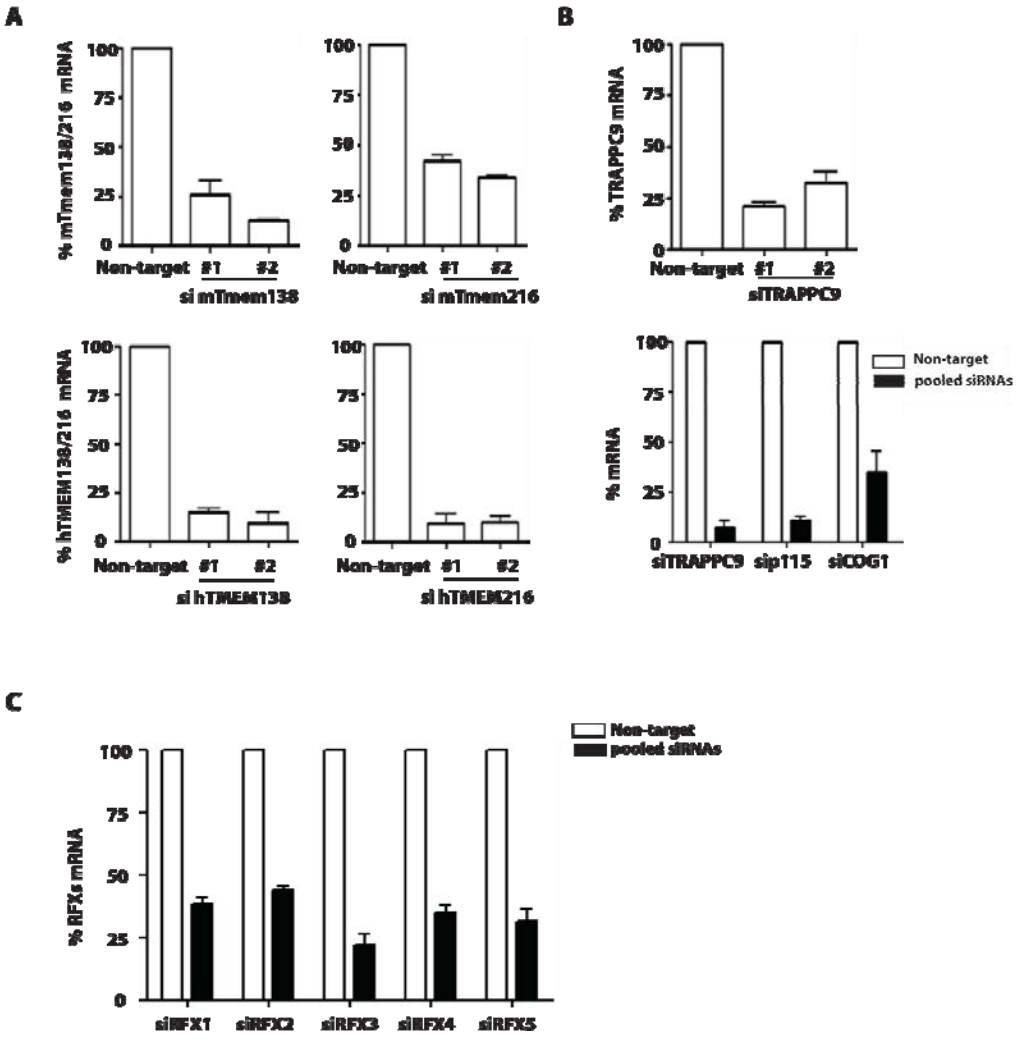

Fig. S19 The knockdown efficiencies of multiple individual or pooled siRNAs used in this study. Using real-time qPCR, the mRNA expressions of targeted genes including mouse or human *TMEM138/216* (A), human *TRAPPC9/p115/COG1* (B), human *RFX1-5* (C) were measured 36-48h after multiple individual or pooled siRNA transfections in IMCD3 (mouse) and hTERT-RPE(human) cells. n=3-4

Table S1. Clinical and molecular data from *TMEM138* mutated families

Family data			Clinical data					Genetic data	
Family	Age(sex)	Origin	CNS	Eye	Kidney	Liver	Other	Nucleotide changes	Protein mutation
MTI-005	2 years(F)	Arab	MTI	OMA,Co	-	-	-	IVS2+5 G>A	splice
	10 years(F)		MTI	OMA,Co	-	-	-		
MTI-002	17 years(M)	Arab	MTI, DWM	OMA	NPH	-	-	A287G	H96R
	Fetus(F)*		Ec						
MTI-381	3 years(F)	Arab	MTI	OMA,Co	CK	-	-	IVS2+5 G>A	splice
	5 years(M)		MTI			-	PD		
	1 deceased (4 years,M)								
MTI-129	24 years(M)	Arab	MTI	RD	-	-	-	C380T	A127V
	23years(M)		MTI	RD	-	-	-		
	22years(M)		MTI	RD	-	-	-		
MTI-656	1 year(F)	Arab	MTI	OMA	-	-	-	G376A	A126T
MTI-499	1 year(F)	Arab	MTI	OMA,Co	CK	-	HYPT	A389G	Y130C
	6 deceased (2M, 4F)								
MTI-998	10 years(M)	Arab	MTI	OMA,Co	-	-	-	G376A	A126T
MTI-1499	2 years(F)	Arab	MTI	OMA,Co	-	-	-	G376A	A126T

Dash (–), not affected; CK, cystic kidneys; Co, chorioretinal coloboma; DWM,Dandy-Walker malformation; Ec, encephalocoele; F, female; HYPT, hypertelorism; M, male; MTI, molar tooth sign on imaging; NPH, nephronophthisis; OMA, oculomotor apraxia; PD, polydactyly; RD,retinal dystrophy; Empty cells denote unavailable clinical information.
*Meckel Syndrome fetus.

Table S2. Chromosomal locations of *TMEM216* and *TMEM138* homologs

Supplemental Table 2. Chromosomal locations of *TMEM216* and *TMEM138* homologs

	Species	Locations*
TMEM138	Homo sapiens	Chr11:61,129,856-61,136,678
	Macaca mulatta	Chr14:12,714,652-12,718,678
	Mus musculus	Chr19:10,645,646-20,649,857
	Monodelphis domestica	Chr5:299,444,527-299,450,474
	Anolis carolinensis	GL343235.1:838,946-844,877
	Xenopus (Silurana) tropicalis	GL17294.2:1,079,78-1,085,419:-1
	Danio rerio	Chr25:3,928,447-3,937,250
TMEM216	Homo sapiens	Chr11:61,159,865-61,166,323
	Macaca mulatta	Chr14:12,690,811-12,698,031
	Mus musculus	Chr19:10,624,956-10,630,728
	Monodelphis domestica	Chr5:299,453,299-299,455,465
	Anolis carolinensis	GL343235.1:852,576-854,425
	Xenopus (Silurana) tropicalis	GL174277.1:1,296-2,573:1
	Danio rerio	Chr14:216,112,867-26,120-163

*Chromosomal locations were obtained from Ensemble Genome Browser

Table S3. Accession numbers of TMEM17, TMEM216, TMEM80, and TMEM138 homologs

	Species	Accession Number
TMEM17	Homo sapiens	NP_938017.2
	Macaca mulatta	XP_001083080.1
	Pan troglodytes	XP_001161917.1
	Bos taurus	NP_001076902.1
	Mus musculus	NP_705824.1
	Rattus norvegicus	NP_001010961.1
	Monodelphis domestica	XP_001382150.1
	Anolis carolinensis	XP_003226867.1
	Xenopus (Silurana) tropicalis	NP_001015683.1
	Danio rerio	NP_001091861.1
	Gasterosteus aculeatus	ENSGACG00000010954
TMEM216	Homo sapiens	NP_001167462.1
	Macaca mulatta	XP_001082614.1
	Bos taurus	XP_870682.2
	Mus musculus	NP_081074.1
	Rattus norvegicus	XP_342021.1
	Monodelphis domestica	XP_001379515.1
	Anolis carolinensis	XP_003224165.1
	Danio rerio	XP_683769.2
	Xenopus (Silurana) tropicalis	XP_002943747.1
TMEM80	Homo sapiens	NP_777600.2
	Pan troglodytes	XP_529374.2
	Macaca mulatta	XP_001087309.1
	Bos taurus	NP_001073781.1
	Mus musculus	NP_082073.1
	Rattus norvegicus	EDM12023.1
	Monodelphis domestica	XP_001379515.1
	Anolis carolinensis	XP_003214886.1
	Xenopus (Silurana) tropicalis	XP_002937534.1
TMEM138	Homo sapiens	NP_057548.1
	Pan troglodytes	XP_508474.2
	Macaca mulatta	XP_001083002.1
	Bos taurus	NP_001092437.1
	Mus musculus	NP_082687.1
	Rattus norvegicus	NP_942072.2
	Anolis carolinensis	XP_003224179.1
	Xenopus (Silurana) tropicalis	NP_001008082.1
	Danio rerio	XP_001333625.1
	Gasterosteus aculeatus	ENSGACG00000005406
	Caenorhabditis elegans	NP_001022074.1
	Drosophila melanogaster	NP_608972.1

Table S4. Protein distance of TMEM138 and TMEM216 homologs

TMEM138 Protein Distance Data

	#AA subs/site[a]	% Identity[b]
Homo sapiens		
P. troglodytes	0.019	96
M. mulatta	0.026	98
B. taurus	0.059	94
M. musculus	0.086	92
R. norvegicus	0.093	91
M. domestica	0.203	83
A. carolinensis	0.164	86
D. rerio	0.414	68
G. aculeatus	0.462	63
X. tropicalis	0.396	70

TMEM216 Protein Distance Data

Homo sapiens		
P. troglodytes	0.007	99
M. mulatta	0.015	99
B. taurus	0.079	93
M. musculus	0.062	93
R. norvegicus	0.071	94
M. domestica	0.272	78
A. carolinensis	0.281	76
D. rerio	0.737	57
G. aculeatus	0.82	49
X. tropicalis	0.677	58

a Protein similarity based on the JTT matrix. Number of amino acid substitutions per site.

b Percent amino acid sequence identity based on Blastp searches at NCBI site.

Table S5. The alignment of TMEM138 homologs

```
                                 1        10        20        30        40        50        60
                                 |        |         |         |         |         |         |
Homo sapiens                     -MLQTSNYSLVLSLQFLLLSYDLFVNSFS-ELLQKTPVIQLVLFI---IQDIAVLFNIII
Pan troglodytes (chimp)          -MLQTSNYSLVLSLQFLLLSYDLFVNSFS-ELLQKTPVIQLVLFMCVHIQDIAVLFNIII
Macaca mulatta (rhesus)          -MLQTSNYSLVLSLQFLLLSYDLFVNSFS-ELLRKAPVIQLVLFI---IQDIAVLFNIII
Bos taurus (cow)                 -MLQTSNYSLVLSLQFLLLSYDLFVNSFS-ELLRMAPVIQLVLFI---IQDIAILFNIII
Mus musculus(mouse)              -MLQTGNYSLVLSLQFLLLSYDLFVNSFS-ELLRMAPVIQLVLFI---IQDIAILFNIII
Rattus norvegicus (rat)          -MLQTSNYSLVLSLQFLLLCYDLFVNSFS-ELLRMAPVIQLVLFI---IQDIAILFNIII
Monodelphis domestica(opossum)    -MLQTSNYSLVLSLQLVLLLYDLLVNAFS-ELLRSAPVVQLVLFI---IQDIAILFNVII
Anolis carolinensis              -MLQTSNYSLVLSLQFLLLSFDLFVNSFS-ELLRMAPVIQLVLFI---IQDIAILFNIII
Xenopus tropicalis               -MLQPGNYSLVLSLQFLLLLFDLFVNSFS-ELLRDPPVNQLVLFI---LQDVGILFAAIV
Danio rerio (zebrafish)          -MLQTNNYSLVLLIQLALLTFDLFVNSFS-ELLRSAPVIQLVLFI---IQDIGILFNVII
G.aculeatus1(stickleback)        -MLQTGNYSLVLLIQMTLLTYDLFVNSFG-ELLRGAPVIQLVLFI---IQDIAILFNVII
G.aculeatus2(stickleback)        ---QTSNYSLVLLIQLSLLSFDLFVNSFS-ELLRHEPAVQLVLFI---IQDISILFNLII
Caenorhabditis briggsae          ---MTSKYPYVLTTQFLMLTIDIFFNALS-ILCYGDNMALLLIYI---LQDTLLIMSSLV
C. elegans                       ---MTSKYPYVLTTQVFMLSIDILFNALG-VLCYGNNMTLLLIYI---LQDTLLIMSSLV
Drosophila melanogaster          MKLTLRRYSWVLLFQFALLGVDLFCNAFGPSLARNRLQTAIILFV---TQDALIIAEYLL

                                61       70        80        90        100       110       120
                                 |        |         |         |         |         |         |

Homo sapiens                     IFLMFFNTFVFQAGLVNLLFHKFKGTIILTAVYFALSISLHVWVMNLRWK--NSNSFIWT
Pan troglodytes                  IFLMFFNTFVFQAGLVNLLFHKFKGTIILTAVYFALSISLHVWVMNLRWK—-NSNSFIWT
Macaca mulatta                   IFLMFFNTFVFQAGLVNLLFHKFKGTIILTAVYFALSISLHVWVMNLRWK--NSNSFIWT
Bos Taurus                       IFLMFFNTFVFQAGLVNLLFHKFKGTIILTAVYFALSISLHVWVMNLRWK--NSNCFVWT
Mus musculus                     IFLMFFNTFVFQAGLVNLLFHKFKGTIILTSVYLALSISLHVWVMNVRWK--NSSSFSWT
Rattus norvegicus                IFLMFFNTFVFQAGLVNLLFHKFKGTIILTSVYLALSISLHVWVMNVRWK--DSSSFRWT
Monodelphis domestica            IFLMFFNTFVFQAGLINLLFRKFKGTIILTAFYLSLSIPLHVWVLNLRWT--DSKHYVWT
Anolis carolinensis              IFLMFFNTFVFQAGLVNLLFHKFKGTIVLSGTYLALSVSFHIWIMNLRWR--SSNYFVWT
Xenopus tropicalis               LFLMLFNTFVFQAGLVSLLCQRFQVTVILCAVYIALSISLHVWLMNLRWT—-GANRFVWS
Danio rerio                      ILLMMFNTYVFQVGLVSLLLERFRAMLILSALYLTLSICFHCWVMNLRWM--ESNRFVWT
Gasterosteus aculeatus1          ILLMMFNTYAFQVGLVSLLLERFRALLIFSAVYLTLSIGFHCWVLNLRWF--ESNRFVWT
Gasterosteus aculeatus2          ILLMLFNTYVFQIGLVAVLLERFRAALMLSALYLTFSIILHSWLMNLRWL--NTNRFIWT
C. briggsae                      LFVSFTATFVFQLGLIHIVLVQFLPTIIMSIFYTFVSIGYHYTSLSSTWED-QTVNIFLE
C. elegans                       LFVSFTATFVFQLGLIHIVIFQFLPTVIISILYTFVSIGYHYASLSSTWED-RTVNIFMN
D. melanogaster                  FTLALHSTCVYQVGASHIILRNCKLFMASITIYFLLSASQHFWIIYQYRQPPEEDGHHWP

                                121      130       140       150       160       170       180
                                 |        |         |         |         |         |         |

Homo sapiens                     DGLQMLFVFQRLAAVLYCYFYKRTAVRLGDPHFYQDSL-WLRKEFMQVRR----------
Pan troglodytes                  DGLQTLFVFQRLAAVLYCYFYKRTAVRLGDPRFYQDSL-WLRKEFMQVRR----------
Macaca mulatta                   DGLQTLFVFQRLAAVLYCYFYKRTAIRLGDPHFYQDSL-WLRKEFMQVRR----------
Bos Taurus                       DGLQTLFVFQRLAAVLYCYFYKRTAVRLGDPRFYQDSL-WLRMEFMQVRR----------
Mus musculus                     NGLQTLFVFQRLAAVLYCYFYKRTAVRLGDPRFYQDSL-WLRKEFMQVRR----------
Rattus norvegicus                NGLQTLFVFQRLAAVLYCYFYKRTAVRLGDPRFYQDSL-WLRKEFMQVRR----------
Monodelphis domestica            DGLQTLFVFQRLAAVLYCYFYKRTAIRLGDPRFYQDSL-WLRKEFTQVRS----------
Anolis carolinensis              DGLQTLFVFQRLAAVLYYYFYKRTAVHLGDPRFYQDSL-WLRKEFAQVRS----------
Xenopus tropicalis               DGLLALFVLQRFVAVLYFYYYKRTALSMGDSRFYHDSL-WLRKEFARVRG----------
Danio rerio                      DGLQVLFVFQRIAAVLYYYFYKRTTEYLGDPRLYEDSP-WLRDAFARARQ----------
Gasterosteus aculeatus1          DGLQALFVFQRTGAVMYYYLYKRTAEYMGDPRLYEDSL-WLREAFARGRQ----------
Gasterosteus aculeatus2          DGLQVLFVFQRVASVLYYYLYKRTSEYLGDPRLYEDSP-WLRELFARHERGSPLPKQK
C. briggsae                      THLLIFFIFHKVISCIFYSFYKRTALQISDPKYNSDST-WLRELFIKHMNDKAAKLEARN
C. elegans                       GPLLLFFIIHKIVSCVFYAYYKRTALQISDPKYNSDST-WLRELFIKHMNDKAAKIEART
D. melanogaster                  LGLIALSVAQRIMSVFYYYSSKSTALTMADPRFKEEHLDWIADQLGDK------------

                                    185
Homo sapiens                     -----
Pan troglodytes                  -----
Macaca mulatta                   -----
Bos taurus                       -----
Mus musculus                     -----
Rattus norvegicus                -----
Monodelphis domestica            -----
Anolis carolinensis              -----
Xenopus tropicalis               -----
Danio rerio                      -----
Gasterosteus aculeatus1          -----
Gasterosteus aculeatus2          SPQNT
C. briggsae                      AAAAT
C. elegans                       AAENN
D. melanogaster                  -----
```

Table S6. The alignment of TMEM80, TMEM216, and TMEM17 homologs

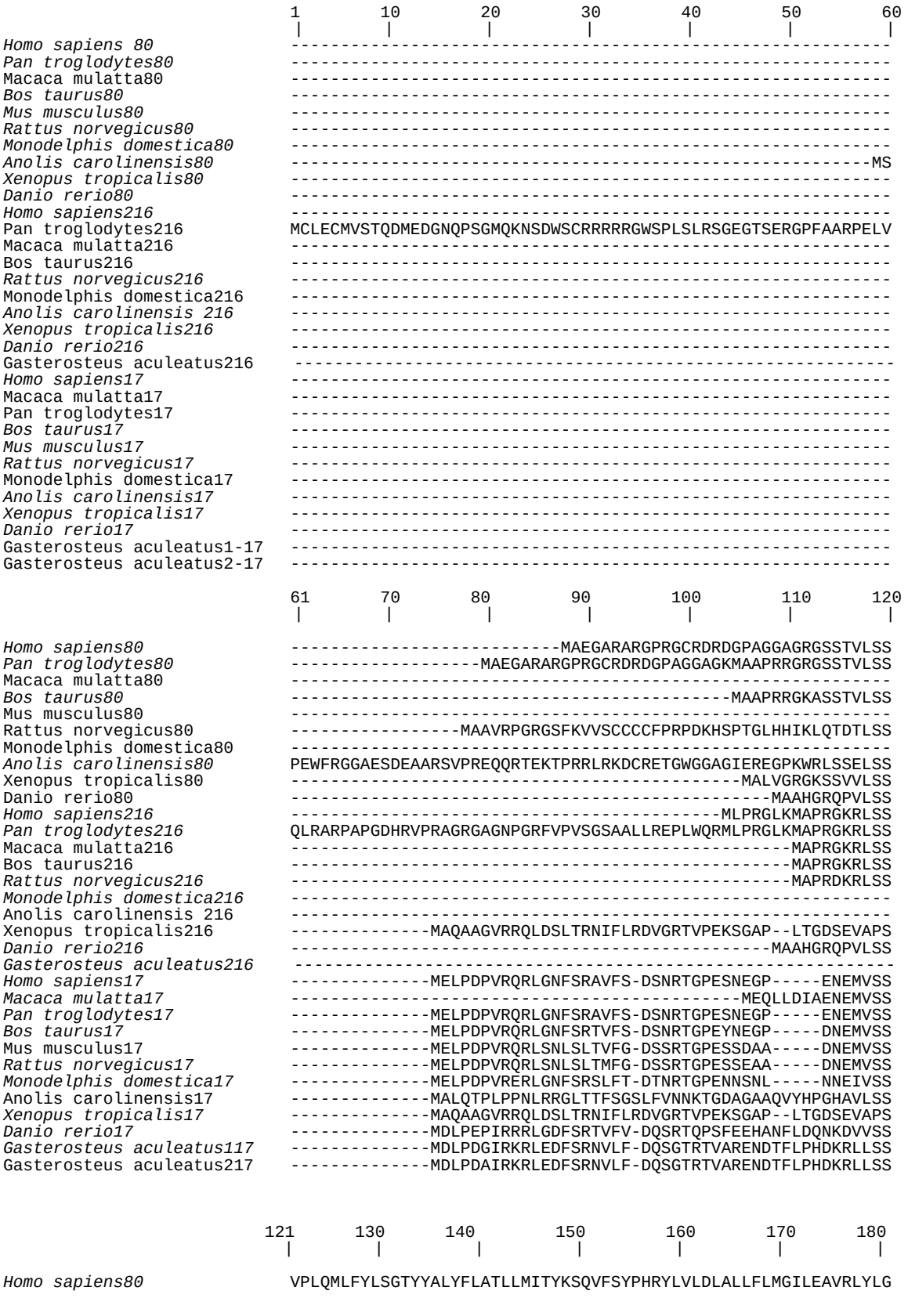

```
Pan troglodytes80            VPLQMLFYLSGTYYALYFLATLLMITYKSQVFSYPHRYLVLDLALLFLMGMLEAVRLYLG
Macaca mulatta80             ----MLFYLSGTYYALYFLATLLMITYKGQVFSCPHHYLVLDLALLFLMGILEALRLYLG
Bos taurus80                 LPLQMLLCLSGTYYALYFLATLLLLVYKSQVFTYPHSCLVLDLTLLFLMGILEAIRLYFG
Mus musculus80               ----MLFHLSGLYSALYFLATLLMIVYKSQVFSYPCNCLALDLVLLLLMGILKVAQLYLG
Rattus norvegicus80          VPLQMLFHLSGLYYALYFLATLLMIVYKSQVFSYPSNCLVLDLVLLLLMGIFEVAQLYLG
Monodelphis domestica80      ------------------------------------------MLFLYLGIEITRIFFG
Anolis carolinensis80        VPLQILFYLNGVYYIFYFFAALLMIIYKSQVFTYPDNFLTLDLILLFIMALLETIRLYFG
Xenopus tropicalis80         VPLQMLLYLNIIYYVFYFLATLLMIIYKSQVFSYPGSNLALDLCLLFLMGILEPVRLYLG
Danio rerio80                TPLQILFHLNGWYFAAFFVAEILMFIYKGVILPYPQDNLILDVVLLLLFSGLETLRLFYG
Homo sapiens 216             TPLEILFFLNGWYNATYFLLELFIFLYKGVLLPYPTANLVLDVVMLLLYLGIEVIRLFFG
Pan troglodytes216           TPLEILFFLNGWYNATYFLLELFIFLYKGVLLPYPTANLVLDVVMLLLYLGIEVIRLFFG
Macaca mulatta216            TPLEILFFLNAWYNATYFLLELFIFLYKGVLLPYPTANLVLDVVMLLLYLGIEVIRLFFG
Bos taurus216                TPLEILFFLNGWYYATYFLLELFIFLYKGLLLPYPTANLVLDVVMLFLYLGVEVIRLFFG
Rattus norvegicus216         TPLEILFFLNGWYYATYFLLELLIFLYKGLLLPYPTANLVLDVVMLLLYLGIEVIRLFFG
Monodelphis domestica216     ------------------------------------------MLFLYLGIEITRIFFG
Anolis carolinensis 216      ------------------------------------------MLFLYLGIEVTRIFFG
Xenopus tropicalis216        VSLQIFLYFNAFYFPFWWVCYVIMLQLKYVLL--PDYYKFILVVLLILMSVIEVIRLYLG
Danio rerio216               TPLQILFHLNGWYFAAFFVAEILMFIYKGVILPYPQDNLILDVVLLLLFSGLETLRLFYG
Gasterosteus aculeatus216    ----VLFYLNSWYFAAFYLAEVLMFIYKGNSLPYPSDNLVLDVVLLVLFLGLEMLRIFYG
Homo sapiens17               LALQMSLYFNTYYFPLWWVSSIMMLHMKYSIL--PDYYKFIVITVIILITLIEAIRLYLG
Macaca mulatta17             LALQMSLYFNTYYFPLWWVSSIMMLHMKYSIL--PDYYKFIVITVIILITLIEAIRLYLG
Pan troglodytes17            LALQMSLYFNTYYFPLWWVSSIMMLHMKYSIL--PDYYKFIVITVIILITLIEAIRLYLG
Bos taurus17                 LALQMSLYFNTYFFPLWWVSSIMMLQMKYSIL--PDYYKFIVVTIIILITLIEAIRLYLG
Mus musculus17               LALQMSLYFNSYFFPLWWVSCIVMLHLKYSIL--PDYYKFIVVTVVILITLIEAIRLYLG
Rattus norvegicus17          LPLQMSLYFNSYFFPLWWVSCIVMLHLKYSVL--PDYYKFIVITVVILITLIEAIRLYLG
Monodelphis domestica17      LALQMSLYFNIYFFPFWWVSSIIMLLLKYPVL--PDYYKFILVTVVILITLIEAIRLYLG
Anolis carolinensis17        LPLQMMLYFNAFYFPFWCLSEGIMLQLKFSLL--PAYNQFLLLSAYLTITLAEVLRLYLG
Xenopus tropicalis17         VSLQIFLYFNAFYFPFWWVCYVIMLQLKYVLL--PDYYKFILVVLLILMSVIEVIRLYLG
Danio rerio17                LPLQMSLYFNMWFFPFWWISEVVMLDLKYSAL--ADYYKFILITILIVMTLIEAIRLYLG
Gasterosteus aculeatus1-17   LHLQMSLYFNMWFFPLWWISEAVMLHLKYPAL--PDYYKFILVTVLILMTLIEAIRLFLG
Gasterosteus aculeatus2-17   LHLQMSLYFNMWFFPLWWISEAVMLHLKYPAL--PDYYKFILVTVLILMTLIEAIRLFLG

                          181      190       200        210        220        230       240
                            |        |         |          |          |          |         |
Homo sapiens80               TRGNLTEAERPLAASLALTAGTALLSAHFLLWQALV--LWADWALSATLLALHGLEAVLQ
Pan troglodytes80            TRGNLTEAERPLAASLALTAGTALLSAHFLLWQTLV--LWADWALSATLLALHSLEAILQ
Macaca mulatta80             TRGNLTEAERPLAASLALTAGTALLSAYFLLWQTLV--LWADWALSATLLALHGLEAVLQ
Bos taurus80                 TTGNLMEAEVPLAASLVLTVGSALLSAYFLLWQTLV--LRADSALGAPLLALHGLEAVLQ
Mus musculus80               TKGNLMEAEVPLAASLAFTAVGGLLSVHFLLWQTLV--LWMDSVLSTVLLVLHGLEAGLQ
Rattus norvegicus80          TQGNLTEAEVPLAASLAFTAVSGLLSVHFLLWQTLV--LWMDSVLSTVLLVLHGLEAGLQ
Monodelphis domestica80      TKGNLCQRMMPLGISLALTFPSAMMASYYLLLQTYV--LRLEAVMGTILLLFCALEVILE
Anolis carolinensis80        TKGNLTEDEAPLGFSLVITAGCVILSVYFLALQTYV--LKADVIINVVLLVIYGLEGILQ
Xenopus tropicalis80         TQGNLAEEEIPLGSSLLVTVGNIFLAIYFLVWQTYI--LRADLIINIILLVIYGLEVILE
Danio rerio80                WKGNLCQRSLALFVSVAILVPCAVLSVYYLLLQTFV--LRLEFVLNAVLLCFYGFELVLG
Homo sapiens216              TKGNLCQRKMPLSISVALTFPSAMMASYYLLLQTYV--LRLEAIMNGILLFFCGSELLLE
Pan troglodytes216           TKGNLCQRKMPLSISVALTFPSAMMASYYLLLQTYV--LRLEAIMNGILLFFCGSELLLE
Macaca mulatta216            TKGNLCQRKMPLSISVALTFPSAMMASYYLLLQTYV--LRLEAIMNGILLFFCGSELLLE
Bos taurus216                TKGNLCQRKMPLGISVALTFPSTMMASYYLLLQTYV--LRLEAIMNSILLFFCGSELLLE
Rattus norvegicus216         TKGNLCQRKMPLGISVALTFPSAMMASYYLLLQTYV--LRLEAIMNSILLFFCGSELLLE
Monodelphis domestica216     TKGNLCQRMMPLGISLALTFPSAMMASYYLLLQTYV--LRLEAVMGTILLLFCALEVILE
Anolis carolinensis 216      SKGNLCQRKVPLAISLALTFPAAVMAAYYLLLQTYA--LRLEAILNAILLLFYAVELLLG
Xenopus tropicalis216        YSGNLQEKVPELAGFCLLSILLQLPLLLFLLCDPGLEPLPLERAVHGILTAFLLIQIPIS
Danio rerio216               WKGNLCQRSLALFVSVAILVPCAVLSVYYLLLQTFV--LRLEFVLNAVLLCFYGFELVLG
Gasterosteus aculeatus216    WKGNLCESSLASCAALLVLLPCAALAVYFLLLQTYV--LRLEFILGAVLLCFYGRELLLG
Homo sapiens17               YVGNLQEKVPELAGFWLLSLLLQLPLILFLLFNEGLTNLPLEKAIHIIFTLFLAFQVVAA
Macaca mulatta17             YMGNLQEKVPELAGFWLLSLLLQLPLILFLLFNEGLTNLPLEKAIHIIFTLFLAFQVVAA
Pan troglodytes17            YVGNLQEKVPELAGFWLLSLLLQLPLILFLLFNEGLTNLPLEKAIHIIFTLFLAFQVVAA
Bos taurus17                 YMGNLQEKVPELAGFWLLSLLLQLPLILFLLFNEGLTNLPLEKAVHIIFTIFLTFQVVSA
Mus musculus17               CMGNLQEKVPELAGFWLLSLLLQLPLILFLLLNDGLRNLPLEKAIHIIFTIFLTFQVISA
Rattus norvegicus17          CMGNLQEKVPELAGFWLLSLLLQLPLLLFLLLNEGLKNLPLEKAIHSIFTVFLTFQVISA
Monodelphis domestica17      YMGNLQEKVPELAGFWLLSFLLQLPLILFLLFNEGLKSQPLERAVHIIFTIFLTLQVVLA
Anolis carolinensis17        YIGNLQEKVPELAGFLLLSLMIEVPTVLFILADMYTLRLPLETAVNLLLLLFLVAEIAAA
Xenopus tropicalis17         YSGNLQEKVPELAGFCLLSILLQLPLLLFLLCDPGLEPLPLERAVHGILTAFLLIQIPIS
Danio rerio17                NAGNLQEKVPELAGFWLLTFLLQFPLILFQLFNEAVLVQPLERGVHIILALFIFAEVLFG
Gasterosteus aculeatus117    YSGNLQEQVPELAGFWLLSILLQFPLILFQLFNEAILIQPLERGVHIVLAIFILAQALSG
Gasterosteus aculeatus217    YSGNLQEQVPELAGFWLLSILLQFPLILFQLFNEAILIQPLERGVHIVLAIFILAQALSG

                          241      250       260        270        280        290       300
                            |        |         |          |          |          |         |
Homo sapiens80               VVAIAAFTR-------------------------------------------------
Pan troglodytes80            VVAIAAFTR-------------------------------------------------
Macaca mulatta80             VVAIAAFTR-------------------------------------------------
Bos taurus80                 VVAIAAFVS-------------------------------------------------
Mus musculus80               VVVIADFIR-------------------------------------------------
Rattus norvegicus80          VVVIADFIR-------------------------------------------------
Monodelphis domestica80      VLTLSTFSSIT-----------------------------------------------
Anolis carolinensis80        IIAIAAFVS-------------------------------------------------
Xenopus tropicalis80         VLTVAAFFRY-----------------------------------------------
Danio rerio80                VMTISIFSRANIY---------------------------------------------
```

```
Homo sapiens 216            VLTLAAFSSMDTI----------------------------------------------
Pan troglodytes216          VLTLAAFSSMDRI----------------------------------------------
Macaca mulatta216           VLTLAAFSSMDRI----------------------------------------------
Bos taurus216               VLTLTAFSSMDR-----------------------------------------------
Rattus norvegicus216        MLTLATFSSMDRI----------------------------------------------
Monodelphis domestica216    VLTLSTFSSIT------------------------------------------------
Anolis carolinensis 216     ILTLAAFS---------------------------------------------------
Xenopus tropicalis216       IFALRKATRHLAGRFHLLGDLDGRA-----------------------------------
Danio rerio216              VMTISIFSRANIY----------------------------------------------
Gasterosteus aculeatus216    LLSIYTFSR-------------------------------------------------
Homo sapiens17              FLTLRKMVNQLAVRFHLQDFDRLSANRGDMRRMRSCIEEI--------------------
Macaca mulatta17            FLTLRKMVNQLAVRFHLQDFDRLSANRGDMRRMRSCIEEI--------------------
Pan troglodytes17           FLTLRKMVNQLAVRFHLQDFDRLSAKRGDMRRMRSCIEEI--------------------
Bos taurus17                FLTLRKMVNQLATRFHLQDFDRLSASRGDMRRVRSCIEEI--------------------
Mus musculus17              FLTLKKMVNQLAARFHLQDFDQLSSSSAAVRRVRQCTEEL--------------------
Rattus norvegicus17         FLTLKKMVNQLAARFHLQDFDQLSASSATGRRARQSSEEL--------------------
Monodelphis domestica17     FFTLKKMANHLAASFQLQDFDRFDQFSSRDMIRAKISTGLENSGHFYLLPAHSPTYTMPT
Anolis carolinensis17       FRALKHMSKQLAMQFYLKQFEEGVGQTPGDGHKGQWVWGS--------------------
Xenopus tropicalis17        IFALRKATRHLAGRFHLLGDLDGRA-----------------------------------
Danio rerio17               FVALRTMVRHTESRFHLRQFHGIQELRT--------------------------------
Gasterosteus aculeatus117   FVTLRDMVRHTGRQFHLRQFD---------------------------------------
Gasterosteus aculeatus217   FVTLRDMVRHTGRQFHLRQFD---------------------------------------

                                                  325
Homo sapiens80              -------------------------
Pan troglodytes80           -------------------------
Macaca mulatta80            -------------------------
Bos taurus80                -------------------------
Mus musculus80              -------------------------
Rattus norvegicus80         -------------------------
Monodelphis domestica80     -------------------------
Anolis carolinensis80       -------------------------
Xenopus tropicalis80        -------------------------
Danio rerio80               -------------------------
Homo sapiens 216            -------------------------
Pan troglodytes216          -------------------------
Macaca mulatta216           -------------------------
Bos taurus216               -------------------------
Rattus norvegicus216        -------------------------
Monodelphis domestica216    -------------------------
Anolis carolinensis 216     -------------------------
Xenopus tropicalis216       -------------------------
Danio rerio216              -------------------------
Gasterosteus aculeatus216   -------------------------
Homo sapiens17              -------------------------
Macaca mulatta17            -------------------------
Pan troglodytes17           -------------------------
Bos taurus17                -------------------------
Mus musculus17              -------------------------
Rattus norvegicus17         -------------------------
Monodelphis domestica17     EAGVLNSLFQNKGNGIFDKNKTFGP
Anolis carolinensis17       -------------------------
Xenopus tropicalis17        -------------------------
Danio rerio17               -------------------------
Gasterosteus aculeatus117   -------------------------
Gasterosteus aculeatus217   ------------------------
```

Table S7. siRNAs, primers, and morpholino antisense oligonucleotides used in this study

siRNAs target sequences
Mouse *TMEM138* siRNA#1 5'-GGGUCAUGAACGUGCGAUG
Mouse *TMEM138* siRNA#2 5'-AGGUUAGCCUGUAGAGAGA

Mouse *TMEM216* siRNA#1 5'-GAACCCAUUUAGUAGUUUA
Mouse *TMEM216* siRNA#2 5'-GUGAAAAGUGGUAGGUCGA

Human *TMEM138* siRNA#1 5'-CAAAGGAUGCGAAGAGUGA
Human *TMEM138* siRNA#2 5'-CAUAUGGACAGAUGGACUU

Human *TMEM216* siRNA#1 5'-GGCAAGCAACUCAGCAUAA
Human *TMEM216* siRNA#2 5'-CCACAUGCUCCCUGUACGA

Human *TRAPPC9* siRNA#1 5'-CGAAAGUUCUCACCACUAA
Human *TRAPPC9* siRNA#2 5'-CCUAUUACAGCAAGUAUAA

Human *RFX1* siRNA pool (5'-CAACACAGGCGUAUACUGA,
UCACAGAGCUCGACCUCCA,
CCGCACAGAUCAACCAGAU,
CCACGUGGCUCAAGAGGUG)
Human *RFX2* siRNA pool (5'-UGACACAGGCCAUCCGUAA,
GAACAGCCUACACCUACAA,
GCACAGCACUCCGGAACAG,
GAGAGACGCCGAUCGCUGU)
Human *RFX3* siRNA pool (5'-GAACAACAACGUAUCCUUA,
GCGAUACUGUCUAUACCAA,
GUAUAUGGCUAUGAGACAA,
CGAAGAUACACGUCGCUUA)

Human *RFX4* siRNA ON-TARGETplus SMARTpool (L-0135577-00-0005, Dharmacon)

Human *RFX5* siRNA ON-TARGETplus SMARTpool (L-011103-00-0005, Dharmacon)

Human *TRAPPC9* siRNA pool (5'-GCAGACGACUGGAACGAUU,
CGAAAGUUCUCACCACUAA,
CCUAUUACAGCAAGUAUAA,
GAAAGUCAGCAACUAAUCA)
Human *p115* siRNA pool (5'-CCAGGGAAGUUAUACGUAA,
AGAAAUUGGUAGAUUGCGA,
GCUCAUAUAUUCAACGUAU,
GUACAAGGAGAGACCGAGA)
Human *COG1* siRNA pool (5'-CCAGGAAAUUAAUCGGGUU,
UGAAGGGUCUCGCGGGAAU,
AACCAGAAACAUCGAAACA,
CUGUAUGGUUCAAGUAGUA)

Primers for quantitative real-time PCR
Mouse *TMEM138* F 5'- CATGAACGTGCGATGGAAAA
Mouse *TMEM138* R 5'- TGTTTGCAGGCCGTTTGTC

Mouse *TMEM216* F 5'- CGTGCTCCGCCTAGAAGCTA
Mouse *TMEM216* R 5'- AGCAGCTCTGAGCCACAAAAG

Human *TMEM138* F 5'- CATCCTGACAGCTGTGTACTTTGC
Human *TMEM138* R 5'- CGTAAGTTCATGACCCAGACATG

Human *TMEM216* F 5'- TGCTGCTGCAGACCTACGTACT
Human *TMEM216* R 5'- CAGAAGAAGAGCAAGATGCCATT

Human *TRAPPC9* F 5'- ACGGTTACCATACCACGGTCTTC
Human *TRAPPC9* R 5'- TTTATTCCCGGCAGGTTATCC

Human *RFX1* F 5'- CCCGAGCGGAGTTGGTAAC
Human *RFX1* R 5'- TGGAACAGATAAGGCCATGATG

Human *RFX2* F 5'- TCACCGGCTCCACCAAAT
Human *RFX2* R 5'- CCCCCGCTTGAGTCAAAGTA

Human *RFX3* F 5'- GCCTCCCCAGCGACAAT
Human *RFX3* R 5'- TGGACAGACCGTCAGACTTTTG

Human *RFX4* F 5'- CCCATGCAGAGCCAGTATCC
Human *RFX4* R 5'- TGGAGTGGCCCAGAGATAGC

Human *RFX5* F 5'- GGCAGGCTCCACCAGCTAA
Human *RFX5* R 5'- TTGGCATCACTTGCTGTATCCT

Human and mouse *b-actin* F 5'- GACCCAGATCATGTTTGAGACC
Human and mouse *b-actin* R 5'- GGCCATCTCTTGCTCGAAGTC

Mouse *36B4* F 5'- GCCAGCTCAGAACACTGGTCTA
Mouse *36B4* R 5'- ATGCCCAAAGCCTGGAAGA

Zebrafish *tmem138* F 5'- CGGAGACCCCAGACTTTACG
Zebrafish *tmem138* R 5'- GCGCTCTTGCGAAAGCAT

Zebrafish *tmem216* F 5'- TGGCTTCGAGCTGGTTCTG
Zebrafish *tmem216* R 5'- AGATGTTGGCCCTGGAAAAA

Zebrafish *Rpl13a* F 5'- GTCTGAAACCCACACGCAAA
Zebrafish *Rpl13a* R 5'- GCCAACTTCATGGGCCAAT

Translational blocking morpholino antisense oligonucleotide for zebrafish *tmem138*
5'-GTAGTTATTTGTCTGGAGCATTTCT

Movie S1. Representative time-lapse sequence of TMEM216-EGFP and dsRed-Centrin2 expressing COS7 cells. TMEM216 tagged vesicles (green) move toward and around the centrosome (red). Images were captured every 3s for 400s . Sacle bar 5um. Selective images from this movie are presented in Fig. S12B.

Movie S2. Representative time-lapse sequence of the fluorescence recovery after photobleaching (FRAP) of EGFP in TMEM216-EGFP and dsRed-Centrin2 expressing COS7 cells. Newly emerging TMEM216 tagged vesicles (green) move toward and around the centrosome (red). The accumulation of GFP signal around the centrosome is shown. Images were captured every 30s for 30min. Sacle bar 5um. Selective images from this movie are presented in Fig. S12B.

Movie S3. Representative time-lapse sequence of TMEM138-EGFP and TMEM216-mCherry expressing COS7 cells. TMEM138 (green) and TMEM216 (red) tagged vesicles move together in a hand-in-hand fashion. Images were captured every 3s for 120s. Scale bar 5um. Selective images form this movie are presented in Fig. 3C.

Movie S4. Representative time-lapse sequence of TMEM138-EGFP and TMEM216-mCherry expressing hTERT-RPE cells. TMEM138 (green) and TMEM216 (red) tagged vesicles move together in a hand-in-hand fashion. Images were captured every 3s for 140s. Scale bar 5um.

Movie S5. Representative time-lapse sequence of TMEM138-EGFP and dsRed-Centrin2 expressing COS7 cells after non-target siRNA transfection. TMEM138 tagged vesicles move toward and around the centrosome. Images were captured every 3s for 120s (9 frames per second). Scale bar 5um. Selective images from this movie are presented in Fig. 4A.

Movie S6. Representative time-lapse sequence of TMEM138-EGFP and dsRed-Centrin2 expressing COS7 cells after siTMEM216 RNA transfection. TMEM216 knockdown disrupts TMEM138 vesicular movement to the centrosome. Images were captured every 3s for 120s (9 frames per second). Scale bar 5um. Selective images from this movie are presented in Fig. 4A.

Movie S7. Representative time-lapse sequence of TMEM138-EGFP and TMEM216-mCherry expressing COS7 cells after non-target siRNA transfection. Non-target siRNAs do not change ‘hand-in-hand fashion’ movements of TMEM138 and TMEM216 labeled vesicles. Images were captured every 3s for 120s. Scale bar 5um. Selective images form this movie are presented in Fig. 4B.

Movie S8. Representative time-lapse sequence of TMEM138-EGFP and TMEM216-mCherry expressing COS7 cells after siTRAPPC9 RNA transfection. TRAPPC9 knockdown detaches tethered TMEM138 and TMEM216 vesicles and inhibited TMEM138 vesicular trafficking. Images were captured every 3s for 120s. Scale bar 5um. Selective images form this movie are presented in Fig. 4B.

Movie S9. Representative time-lapse sequence of TMEM138-EGFP and TMEM216-mCherry expressing COS7 cells after sip115 RNA transfection. Images were captured every 3s for 120s. Scale bar 5um.

Movie S10. Representative time-lapse sequence of TMEM138-EGFP and TMEM216-mCherry COS7 cells after siCOG1 RNA transfection. Images were captured every 3s for 120s. Scale bar 5um

Movie S11. Representative time-lapse sequence of tmem138-EGFP and tmem216-mCherry expressing ZF4 (zebrafish embryonic fibroblasts) cells. Images were captured every 3s for 120s. Scale bar 5um.

References

1. E. Birney *et al.*, *Genome Res* **14**, 925 (2004).
2. I. Ovcharenko, M. A. Nobrega, G. G. Loots, L. Stubbs, *Nucleic Acids Res* **32**, W280 (2004).
3. K. A. Frazer, L. Pachter, A. Poliakov, E. M. Rubin, I. Dubchak, *Nucleic Acids Res* **32**, W273 (2004).
4. A. Siepel *et al.*, *Genome Res* **15**, 1034 (2005).
5. E. Birney *et al.*, *Nature* **447**, 799 (2007).
6. A. Visel, S. Minovitsky, I. Dubchak, L. A. Pennacchio, *Nucleic Acids Res* **35**, D88 (2007).
7. L. Kall, A. Krogh, E. L. Sonnhammer, *Nucleic Acids Res* **35**, W429 (2007).
8. T. A. Hall, *Nucleic Acids Symposium Series* **41**, 95 (1999).
9. K. Tamura, J. Dudley, M. Nei, S. Kumar, *Mol Biol Evol* **24**, 1596 (2007).
10. E. M. Valente *et al.*, *Nat Genet* **42**, 619 (2010).
11. A. Yamasaki *et al.*, *Mol Biol Cell* **20**, 4205 (2009).
12. A. M. Ashique *et al.*, *Sci Signal* **2**, ra70 (2009).
13. K. Rogowski *et al.*, *Cell* **143**, 564 (2010).
14. T. Caspary, C. E. Larkins, K. V. Anderson, *Dev Cell* **12**, 767 (2007).
15. J. Kim, S. R. Krishnaswami, J. G. Gleeson, *Hum Mol Genet* **17**, 3796 (2008).
16. S. S. Trueba *et al.*, *J Clin Endocrinol Metab* **90**, 455 (2005).
17. Y. W. Cho *et al.*, *Cell Metab* **10**, 27 (2009).
18. R. Araki *et al.*, *J Biol Chem* **279**, 10237 (2004).
19. N. D. Heintzman *et al.*, *Nat Genet* **39**, 311 (2007).
20. B. P. Piasecki, J. Burghoorn, P. Swoboda, *Proc Natl Acad Sci U S A* **107**, 12969 (2010).
21. B. Craige *et al.*, *J Cell Biol* **190**, 927 (2010).
22. G. H. Mochida *et al.*, *Am J Hum Genet* **85**, 897 (2009).
23. M. Safran *et al.*, *Database (Oxford)* **2010**, baq020.
24. L. Baala *et al.*, *Am J Hum Genet* **80**, 186 (2007).